Mapping drug-microenvironment-genetic interplay in CLL reveals trisomy 12 as a modulator of microenvironmental signals

Short Title for Running Head:

Drug-microenvironment-genetic interplay in CLL

Peter-Martin Bruch*[1,2], Holly A. R. Giles*[1-4], Carolin Kolb[1,2], Sophie A. Herbst[1-3,5], Tina Becirovic[1], Tobias Roider[1-3], Junyan Lu[3], Sebastian Scheinost[5,7], Lena Wagner[5,7], Jennifer Huellein[3], Ivan Berest[3], Mark Kriegsmann[6], Katharina Kriegsmann[1], Christiane Zgorzelski[6], Peter Dreger[1], Judith B. Zaugg[2,3], Carsten Müller-Tidow[1,2], Thorsten Zenz[8], Wolfgang Huber*[2,3], Sascha Dietrich*[1-3,5]

*These authors contributed equally.

1. Department of Medicine V, University of Heidelberg, Heidelberg, Germany
2. Molecular Medicine Partnership Unit (MMPU), Heidelberg, Germany
3. EMBL Heidelberg, Heidelberg, Germany
4. Collaboration for joint PhD degree between EMBL and Heidelberg University, Faculty of Biosciences, Heidelberg, Germany
5. German Cancer Research Center (DKFZ), Heidelberg, Germany
6. Institute of Pathology, University of Heidelberg, Heidelberg, Germany
7. National Center for Tumour Diseases, Heidelberg, Germany
8. Department of Hematology, University of Zürich, Zürich, Switzerland

Corresponding Author Details

Name: Sascha Dietrich

Address: Im Neuenheimer Feld 410, 69120 Heidelberg, Germany

Email: Sascha.Dietrich@med.uni-heidelberg.de

Phone: 06221/56-39894 06621/56-310977

Fax number: 06221/56-5736

Name: Wolfgang Huber

Address: Meyerhofstraße 1, 69117 Heidelberg, Germany

Email: wolfgang.huber@embl.de

Phone: +49 6221 387-8823

Fax number: +49 6221 387-8166

Presented in abstract form at the 61st annual meeting of the American Society of Hematology, Orlando, FL, 13 November 2019[1]**.**

Key Points:

1) The tumour microenvironment has distinct effects in patient subgroups and modulates drug sensitivity and CLL proliferative capacity.
2) Systematic dataset identifies trisomy 12 and JAK-STAT signalling as important players in cell-extrinsic drug resistance mechanisms.

Abstract

The tumour microenvironment and gene mutations collectively influence drug efficacy in Chronic Lymphocytic Leukaemia (CLL), however an integrative understanding of their interplay is missing. We performed a combinatorial assay using 12 drugs individually co-applied with each of 17 microenvironmental stimuli in 192 primary CLL samples, generating a comprehensive map of drug-microenvironment interactions in CLL. We combined our data with whole-exome sequencing, DNA-methylation, RNA-sequencing and copy number variant data. We complemented these experiments by staining healthy and CLL-infiltrated lymph nodes for downstream mediators of key microenvironmental pathways. Our assay identified four distinct CLL subgroups that differed in their responses to the panel of stimuli and in patient outcomes, distinct from known prognostic groups. Additionally, we identified trisomy 12 as an amplifier of responses to the stimuli, mediated by the transcription factors Spi-B and PU.1. We quantified the impact of the stimuli on drug response, distinguished antagonistic and synergistic combinations and characterised their dependency on genetic alterations. The most frequent modulators of drug responses were stimuli activating Interleukin (IL) 4 and Toll-Like Receptor 7/8/9 signaling. Both pathways were more active in CLL-infiltrated lymph nodes than in healthy samples ($p<0.001$), and high IL4 activity in lymph nodes correlated with shorter survival ($p=0.038$). We provide a publically-available resource to investigate microenvironmental, genetic and drug interplay in CLL. Our results highlight the importance of tumour cell extrinsic influences on drug response and disease progression, and how these are further modulated by cell intrinsic molecular features.

Introduction

CLL is a common B-cell malignancy, attributed to the accumulation of mature B-lymphocytes in the peripheral blood, bone marrow, and lymph nodes[2]. The disease course is heterogeneous, influenced by multiple factors including B cell receptor (BCR) signalling, genetic alterations, epigenetic effects and the tumour microenvironment[3]. Despite significant improvements to CLL treatment, including the advent of BCR inhibitors[4] and BH3-mimetics[5], CLL remains incurable. There is a compelling need to better understand cell-intrinsic and extrinsic causes of therapy failure.

The genetic landscape of CLL is well characterised. The most important features include del(17p), *TP53*-mutations, immunoglobulin heavy chain gene (IGHV) mutation status, del(13q) and trisomy 12[6,7]. This list of recurrent genetic and structural alterations has expanded in the past years[8], and is increasingly being used for treatment stratification.

Additionally to cell-intrinsic factors, CLL cell proliferation and survival is dependent on the lymph node microenvironment[9], which is underlined by the observation that CLL cells undergo spontaneous apoptosis *in vitro* if deprived of these signals[10]. Microenvironmental stimuli can induce drug resistance in vitro, for example, the combination of IL2 and Toll-Like Receptor (TLR) stimulation induces resistance to venetoclax[11]. The CLL microenvironment constitutes a complex network of stromal and immune cells that promote cell expansion[12] via soluble factors and cell-cell contacts. Microenvironmental signaling is particularly important in protective niches, especially lymph nodes. Incomplete response to BCR inhibitors has been linked to persistent enlargement of lymph nodes[13], which are the main site of CLL proliferation[9].

Several studies have investigated individual components of the microenvironment in leukaemia[14–18]. However systematic studies, particularly those exploring cell-extrinsic influences on drug response, are rare. Carey et al.[19] have screened acute myeloid leukemia samples with a panel of soluble factors and among them identified IL1ß as a mediator of

cellular expansion in Acute Myeloid Leukemia. This example highlights the value of systematic approaches to dissect tumour-microenvironment cross-talk.

Taking this approach further, we screened a panel of microenvironmental stimuli in CLL, individually and in combination with drugs, and complemented our dataset with multi-omics data on the patient samples. In this study, we integrate genetic, epigenetic and microenvironmental modulators of drug response in CLL systematically in a large patient cohort that covers the clinical and molecular diversity of CLL. Layer by layer, we develop an integrative understanding of the pathways underlying survival and drug efficacy in CLL.

Methods

Sample preparation and drug-stimulation profiling

Sample preparation, cell-culture, drug-stimulation profiling and genomic annotation was performed on 192 CLL patient samples as previously described[20] with the following adjustments. Stimuli and drugs were mixed and preplated in the culture plates directly before adding the cell suspensions. RPMI-1640 and supplements were acquired from Gibco by Life Technologies, human serum was acquired from PAN Biotech (Cat.No. P40-2701, Lot.No:P-020317). Luminescence was measured after 48h on a Perkin Elmer EnVision.

Compounds and Stimuli

Compounds and stimulatory agents were dissolved, stored and diluted according to manufacturer's protocol. HS-5 conditioned medium was produced by incubating HS-5 stromal cell line to >80% confluency and cell removal by centrifugation. For a detailed list of stimuli and drugs and associated concentrations see Supp. Tables 1 and 2. Final DMSO concentration did not exceed 0.3%.

Spi-B and PU.1 shRNA Knockdown

shRNAs directed against PU.1 (shRNA: 5'-GAAGAAGCTCACCTACCAGTT-3')[21] and Spi-B (shRNA: 5'-CAAGGTTCCCTCTTGTCAGAT-3')[22] were integrated into the pLKO.1 vector backbone (Addgene plasmid #10878) according to the manufacturer's protocol using pLKO.1-scramble shRNA (Addgene plasmid #1864) as control.

Lentiviruses were produced by co-transfecting psPAX2 (4.8 µg; Addgene plasmid #12260), pMD2.G (3.2 µg; Addgene plasmid #12259) and one of the cloned shRNA plasmids (8 µg) to HEK 293T cells. Virus-containing medium was collected 48 and 72 h post transfection and concentrated via ultracentrifugation. The target cells were transduced in 96-well plates and sufficient amounts of virus were added to transduce about 80% of the cells. Spinoculation was performed in the presence of polybrene (SU-DHL 4, SU-DHL 5: 8 µg/mL; SU-DHL 2: 12 µg/mL) for 45 min at 3,200g. At 72h post infection, the cells were selected with puromycin (0.5 µg/mL).

For the PU.1/Spi-B Double-KD, the Spi-B-KD cell lines were additionally transduced with the PU.1-KD lentivirus in the same manner as in the first transduction. Knockdown efficiencies were confirmed by PU.1 and Spi-B western blots.

Immunohistochemistry

Lymph node biopsies of CLL-infiltrated and non-neoplastic samples were formalin fixed and paraffin embedded, arranged in Tissue Microarrays and stained for pSTAT6 (ab28829, Abcam) and pIRAK4 (ab216513, Abcam). The slides were analysed using Qupath[23] and the recommended protocol.

Data processing and statistical analysis

To quantify the responses to drugs and stimuli, we used a measure of viability relative to the control, namely the natural logarithm of the ratio between CellTiter Glo luminescence readout of the respective treatment and the median of luminescence readouts of the DMSO control wells on the same plate, excluding controls on the outer plate edges. Data analysis was performed using R version 4 and using packages including DESeq2[24], survival[25], Glmnet[26], ConsensusClusterPlus[27], clusterProfiler[28], ChIPseeker[29], genomation[30] and BloodCancerMultiOmics2017[31] to perform univariate association tests, multivariate regression with and without lasso penalization, Cox regression, generalised linear modelling and clustering. The complete analysis is described along with computer-executable transcripts at github.com/Huber-group-EMBL/CLLCytokineScreen2021.

ATACseq analysis

For Fig 4B, we selected the raw sequencing files from Rendeiro et al. 2016[32] to include one sample per patient passing quality checks (n=52). We obtained bam files mapped to the hg19 genome, adjusted for CG bias, as previously outlined[33]. As trisomy 12 status was not already annotated, we called trisomy 12 in samples that contained > 1.4 times more reads per peak on average in chromosome 12, compared to peaks on other chromosomes. We used diffTf in permutation mode[33] to investigate differential TF activity between trisomy 12 and non-trisomy

12 samples using HOCOMOCO v10[34] and with design formula: "~ sample_processing_batch + sex + IGHV status + trisomy 12".

Data Sharing Statement

Screening data and patient annotation used in this study are available at github.com/Huber-group-EMBL/CLLCytokineScreen2021. For original sequencing data and raw viability data please contact the corresponding authors. We obtained CLL ATACseq data[32] from the EGA (EGAD00001002110) and ChIPseq data for Spi-B binding[35] from the NCBI GEO database[36] (GSE56857, GSM1370276).

Results

Ex-vivo cell viability assay demonstrates functional diversity of cytokine and microenvironmental signalling pathways

We measured the effects of 17 cytokines and microenvironmental stimuli on cell viability in 192 primary CLL samples and combined each with 12 drugs to investigate the influence on spontaneous and drug-induced apoptosis. (Fig 1A-C, Supp. Tables 1 -3). Viability was assessed by ATP measurement after 48h and normalised to untreated controls[20].

The patient samples were characterised by DNA sequencing, mapping of copy number variants, genome-wide DNA-methylation profiling, and RNA-Sequencing[20]. The distribution of genetic features in our cohort is comparable to other studies (Supp. Fig 1)[7].

To assess the heterogeneity of the response patterns, we calculated Pearson correlation coefficients for each pair of drugs and each pair of stimuli. For the drugs, high correlation coefficients (>0.75) were associated with identical target pathways. For example, drugs targeting the BCR pathway (ibrutinib, idelalisib, PRT062607 and selumetinib) were highly correlated, indicating that our data sensitively and specifically reflect interindividual differences in pathway dependencies (Fig. 1D)[20].

In contrast, microenvironmental stimuli showed lower correlations, even where stimuli targeted similar pathways (Fig. 1E, Supp. Fig. 2). For example, lower correlations were observed between different stimuli of the JAK-STAT and NfκB pathways, indicating a low degree of redundancy between stimuli. High correlations (R>0.75) were only seen with the TLR stimuli Resiquimod (TLR7/8) and CpG ODN (TLR9) as well as IL4 and IL4 + soluble CD40L (sCD40L), which target near identical receptors and downstream targets.

Most stimuli increased CLL viability, underlining the supportive nature of the microenvironment. However, IL6, tumor growth factor β (TGFβ) and TLR7/8/9 agonists in IGHV-mutated (IGHV-M) samples decreased viability (Supp. Fig. 3). The strongest responses

were seen with IL4 and TLR7/8/9 agonists, highlighting the potency of these pathways in modulating CLL survival. All screening data can be explored manually (github.com/Huber-group-EMBL/CLLCytokineScreen2021) and interactively, via the shiny app (imbi.uni-heidelberg.de/dietrichlab/CLL_Microenvironment/).

Patterns of responses to microenvironmental stimuli reveal two subgroups of IGHV-M CLL with differential aggressiveness

To gain a global overview over the pattern of responses to our set of microenvironmental stimuli across patient samples, we clustered[27] and visualised the response profiles (Fig. 2A).

This analysis revealed four functionally-defined subgroups with distinct response profiles. Two clusters (termed C1 & C2) were enriched in IGHV-Unmutated (IGHV-U), two (C3 and C4) in IGHV-M CLL. C1 and C2 showed strong responses to IL4 and TLR7/8/9 agonists. C2 was distinguished by stronger responses to the stimuli overall, in particular to NFκB agonists including IL1β and anti-IgM. C3 responded weakly to the majority of stimuli, while C4 was defined by a decreased viability upon TLR7/8/9 stimulation (Supp Fig. 4).

Next, we investigated whether these clusters were associated with differential *in vivo* disease progression of the corresponding patients. We used lymphocyte doubling time and time to next treatment to quantify the proliferative capacity of CLL cells. In line with clinical observations[37], the IGHV-U enriched C1 and C2 showed a shorter lymphocyte doubling time than the IGHV-M enriched C3 and C4. More strikingly, C3 showed a significantly shorter lymphocyte doubling time than C4, indicating a higher proliferative capacity (Fig. 2B).

This observation was reflected in disease progression rates: The predominantly IGHV-M C3 showed a progression dynamic similar to the IGHV-U enriched C1 and C2. C4 however showed a longer time to next treatment than C1, C2 and C3 (Cox proportional hazards model, $p= 0.0014$, <0.001, 0.005 respectively, Fig. 2C, Supp. Fig 5A&B). This points towards a subset

of mostly IGHV-M patients with more aggressive disease, which is characterized by its differential response to microenvironmental stimuli.

To characterise genetic differences between clusters, we calculated predictor profiles for cluster assignment, using multinomial regression with the sample mutation profiles (Fig. 2D). IGHV status was the main predictor of all clusters. Trisomy 12 and *SF3B1* mutations were enriched in C2, which showed enhanced responses to many stimuli. C4, which was associated with slow *in vivo* progression, showed depletion of *TP53*, *ATM*, *RAS*/*RAF* mutations and gain(8q).

The observed difference in progression dynamics *in vivo* was not explained solely by the known prognostic markers IGHV, trisomy 12, and *TP53*. A multivariate Cox proportional hazards model accounting for these features showed an independent prognostic value of the cluster assignment between C3 and C4 (p=0.039, Supp. Table 4).

To examine why C3 exhibited faster disease progression than C4, we compared baseline pathway activity at the time of sampling, using RNA-Sequencing (Supp. Fig. 6A). Gene set enrichment analysis revealed that key cytokine gene sets were upregulated in C3, including TNFα signaling via NFκB, indicating higher pathway activity *in vivo* (Fig. 2E, Supp. Fig. 6B). In addition, pathways that indicate more aggressive disease relating to proliferation, metabolism and stress response, were upregulated in C3 (Supp. Fig. 6 C-E).

Taken together, the patterns of responses to our set of stimuli distinguish two subgroups of IGHV-M CLL (C3 and C4) that are characterized by distinct *in vivo* pathway activities and differential disease progression.

Microenvironmental signals and genetic features collectively determine malignant cell survival

Having observed heterogeneous responses to stimulation, we performed univariate analyses of genetic determinants of stimulus response, including IGHV status, somatic gene mutations, and structural variants (Fig. 3A). We identified at least one genetic feature determined stimulus response for 10/17 stimuli and ≥2 features for 6/17 stimuli (Student's t-tests, FDR = 10%), indicating that CLL viability is controlled both by cell-intrinsic mutations and the cells' microenvironment. The most prominent factors were IGHV status and trisomy 12. Responses to microenvironmental stimuli were largely independent of receptor expression (Supp. Fig. 7).

To address the possible interplay of multiple genetic factors, we applied linear regression with lasso regularisation to derive for each stimulus a multivariate predictor composed of genetic, IGHV and DNA methylation covariates (Fig. 3B). This revealed at least one genetic predictor for five of the 17 stimuli. Trisomy 12 and IGHV status were again the most common features. Stimulus responses stratified by mutations, along with regression model fits can be explored online.

Trisomy 12 is a key modulator of responses to stimuli

Our survey of genetic determinants of stimuli response highlighted trisomy 12 as a modulator of responses to IL4, TGFβ, soluble CD40L + IL4 and TLR stimuli.

TLR response has previously been shown to depend on the IGHV mutation status[17]; we identified trisomy 12 as a second major determinant of response to TLR stimulation. Among the samples without trisomy 12, those with unmutated IGHV displayed increased viability upon TLR stimulation, whereas the response of IGHV-M samples was more heterogeneous, ranging from a strong decrease to a slight increase in viability. In contrast, trisomy 12 samples in both IGHV-U and M cases responded to TLR agonists with increased viability (Student's t-test, $p<0.001$ and $p=0.018$, Fig. 4A).

To investigate the incompletely understood role of trisomy 12 in CLL we investigated how it might modulate responses to cell-extrinsic signals. We investigated transcription factor (TF) activity in trisomy 12 CLL using two independent ATAC sequencing datasets and used *diffTF*[33] to identify TFs with differential binding site accessibility. The first, produced by ourselves, comprised two WT and two trisomy 12 samples; the second, taken from Rendeiro et al., included 43 WT and nine trisomy 12 samples. The binding sites of 92 and nine TFs respectively were more accessible ($p<0.05$) in the trisomy 12 samples (Fig. 4B, Supp. Fig. 8), reflecting a specific signaling signature in trisomy 12 CLL. In both datasets, the top hits were the hematopoietic regulators Spi-B and/or PU.1, which share similar binding motifs and exhibit functional redundancy[38]. These TFs are known to be key regulators of healthy B-cell function[39,40], controlling B-cell responses to environmental cues including CD40L, TLR ligands and IL4[41].

To investigate Spi-B and PU.1 activity in lymphoma, we hypothesised that these TFs may modulate proliferation by coordinating transcriptional response to microenvironmental signals. To identify Spi-B and PU.1 target genes, we reanalysed a ChIPseq dataset[35], quantifying binding in lymphoma cell lines and tested functional enrichment of immune signalling pathways amongst Spi-B and PU.1 targets. Using selected KEGG and Reactome genesets, we found that TLR, BCR and TGFβ signalling genes were enriched ($p<0.01$) amongst Spi-B and PU.1 targets (Fig. 4C).

We next investigated the impact of inhibition of Spi-B and PU.1 on proliferation (Fig. 4D). We generated single and double shRNA knockdowns (due to functional redundancy between the TFs) in lymphoma cell lines, both with (SU-DHL4, SU-DHL5) and without trisomy 12 (SU-DHL2) and measured cell proliferation by cell counts every 24 hours. Single knockdown of Spi-B reduced the proliferation rate in SU-DHL5, whilst the PU.1 single knockdown had a smaller impact. Double KD of Spi-B and PU.1 reduced the proliferation in SU-DHL2 and SU-DHL4, and was lethal in SU-DHL5.

Taken together, we show trisomy 12 is a modulator of response to microenvironmental signals, and link trisomy 12 to higher activity of Spi-B and PU.1, which regulate genes relating to environmental sensing.

Mapping drug-microenvironment interactions reveals drug resistance and sensitivity pathways

Guided by the observation of reduced treatment efficacy in protective niches[13], we examined the effects of the stimuli on drug response.

We fitted a linear model (Eqn 1) to quantify how each stimulus modulates drug efficacy beyond its individual effects, such as the impact of the stimuli on baseline viability and spontaneous apoptosis. β_{int}, termed the interaction factor, quantifies how the combined treatment effect differs from the sum of the individual treatment effects.

$$\log V = \beta_d X_d + \beta_s X_s + \beta_{int} X_d X_s + \varepsilon \qquad \text{Eqn 1}$$

V represents the viability with a given treatment, β_d, β_s and β_{int} are coefficients for the drug, stimulus and combinatorial terms and X_d and X_s are indicator variables (0 or 1) for the presence or absence of a drug/stimulus. ε is the vector of model residuals.

45 out of 204 combinations had a β_{int} with $p<0.05$. We classified these into four categories, based on the sign of β_{int} and whether the combination effect was antagonistic or synergistic (Fig. 5A-C).

Positive antagonistic interactions were the most common category, in which stimuli reversed drug action and increased viability. These interactions could lead to treatment resistance *in vivo*. They comprised known resistance mechanisms including the inactivation of ibrutinib by

IL4 signalling (Fig. 5D)[15], and previously unknown resistance pathways, notably the effect of Interferon-γ (IFNγ) signalling on ibrutinib response (Fig. 5E).

6/45 interactions were categorised as negative antagonistic, in which drug action reversed the pro-survival effect of microenvironmental stimulation. These interactions point to strategies to overcome treatment resistance. For instance, Pan-JAK inhibition reduced the increase in viability from sCD40L + IL4 stimulation (Fig. 5F).

We observed a single positive synergistic case, whereby simultaneous treatment with IFNγ and ralimetinib, a p38 MAPK inhibitor, induced a synergistic increase in viability which was not observed with either single treatment (Fig. 5G), pointing towards an inhibitory effect of p38 activity on IFNγ signalling.

16 combinations showed negative synergistic interactions. For example, TLR9 agonist CpG ODN increased the efficacy of BCR inhibition (Fig. 5H). Interestingly, in samples where TLR stimulation increased viability, the addition of BCR inhibitors (ibrutinib and idelalisib) suppressed this effect, indicating that the increase of viability upon TLR stimulation is dependent on BCR activity. The efficacy of luminespib, a HSP90 inhibitor, increased with various stimuli, including soluble anti-IgM (Fig. 5I).

Altogether, these results highlight the influence of the microenvironment on drug efficacy and underline the value of microenvironmental stimulation in *ex vivo* studies of drug efficacy.

Genetic features affect drug-microenvironment interactions

Next, to investigate to what extent genetic driver mutations modulated the interactions between stimuli and drugs, we fit the linear model in Eqn. (1) in a sample - specific manner.

This resulted in a sample-specific β_{int} interaction coefficient for each drug - stimulus combination. We looked for associations between the size of β_{int} and genetic features using multivariate regression with L1 (lasso) regularisation, with gene mutations and IGHV status as predictors. We generated a predictor profile for each drug - stimulus combination, considering predictors that were selected in >90% of bootstrapped model fits. In total, we found genetic modulators for 60/204 interactions (Fig 6A, Supp Fig. 9). Trisomy 12 and IGHV status modulated the largest number of interactions.

For example, we found the value of β_{int} for fludarabine and CpG ODN to be modulated by six genetic factors; most strongly by IGHV status, del(11q) and trisomy 12 (Fig. 6B).
In IGHV-M non-trisomy 12 samples, fludarabine efficacy increased in the presence of TLR stimulation, whilst in the other subgroups TLR stimulation induced resistance to fludarabine (Fig. 6C).

Our approach also identified interactions dependent on single treatment effects. IL4 induced complete resistance to ibrutinib regardless of higher ibrutinib efficacy in trisomy 12 and IGHV-U samples. This highlights the breadth of IL4-induced resistance to ibrutinib in CLL across genetic backgrounds (Fig. 6D, Supp. Fig. 10).

Overall these findings illustrate how the presence of known genetic alterations determines how drugs and external stimuli interact with each other.

The key resistance pathways IL4 and TLR show increased activity in CLL-infiltrated lymph nodes

Microenvironmental signalling within lymph nodes has been implicated in treatment resistance[9,42–44], though a clear understanding of the mechanisms involved remains missing. Since IL4 and TLR signalling were the most prominent modulators of drug response in our

study, we assessed their activity within the lymph node niche. We stained paraffin embedded sections of 100 CLL-infiltrated and 100 non-neoplastic lymph nodes for pSTAT6, an essential downstream target of IL4 (Supp. Fig. 11), and pIRAK4, a downstream target of TLR7/8/9.

The CLL-infiltrated lymph nodes showed higher levels of pSTAT6 (Fig. 7A) and pIRAK4 (Fig. 7B). Examples are shown in Fig. 7C-F.

To investigate the influence of microenvironmental activity in lymph nodes on CLL disease progression, we correlated staining intensity to treatment free survival. High activity of pSTAT-6 correlated with shorter treatment free survival (Fig. 7G), the same trend could be observed with higher pIRAK4 (Fig. 7H).

Discussion

Our work maps the effects of microenvironmental stimuli in the presence of drugs and links these to underlying molecular properties across 192 primary CLL samples. We employ all combinations of 17 stimuli with 12 drugs as a reductionist model of microenvironmental signalling. We account for the confounding effects of spontaneous apoptosis *ex vivo* and dissect the effect of individual microenvironmental stimuli on baseline viability and drug toxicity. The results may serve as building blocks for a more holistic understanding of the interactions of tumour genetics, microenvironment and drug response in complex *in vivo* situations.

We discover that CLL subgroups can be extracted from microenvironmental response phenotypes and that this classification is linked to distinct molecular profiles and clinical outcomes. IGHV-M samples with weaker responses to microenvironmental stimuli showed faster disease progression, highlighting the important role microenvironmental signalling may play in CLL pathophysiology.

The sensitivity afforded by our approach enabled us to identify drug - stimulus interactions, meaning instances where the effect of a drug on the tumour cells is modulated by a microenvironmental stimulus. Our assay recapitulated known drug-resistance phenomena, such as the impact of IL4 stimulation on ibrutinib and idelalisib[15] and identified new ones, including IFNγ-induced resistance to BCR inhibition. Systematic mapping of drug-stimulus interactions, such as generated in this study, can be used to inform biology-based combinatorial treatments across different entities.

We demonstrated the breadth of IL4-induced resistance against kinase inhibitors and chemotherapeutics across a range of genetic backgrounds. IL4 induced complete resistance to BCR inhibitors across genetic subgroups, despite greater BCR inhibitor efficacy in IGHV-U CLL. Further, we observed increased IL4 activity within CLL-infiltrated lymph nodes and the association of higher activity with faster disease progression. Our work highlights the significance of IL4 within the lymph node niche, especially since proliferation[9] and resistance to BCR inhibition[13] is linked to lymph nodes and our recent work suggests T follicular helper

cells as a source of IL4[45]. Targeting pathways downstream of IL4, via JAK inhibition, has been reported to improve BCR response in non-responding CLL patients[46].

Underneath cell-extrinsic factors that control the apoptotic and proliferative activity of tumour cells in response to drugs there lies the network of cell-intrinsic molecular components. We used multivariate modelling to capture the impact of molecular features on responses to stimuli and drugs. For instance, the response to TLR stimulation depended on IGHV status, trisomy 12, del11q, del13q and ATM, reflecting the multiple layers of biology involved. Most strikingly, we observed that TLR stimulation increased fludarabine toxicity in the subgroup of IGHV-M non-trisomy 12 patient samples, while it led to fludarabine resistance in all other backgrounds. This finding, combined with our observation that TLR signalling is highly active in CLL-infiltrated lymph nodes might help explain the heterogeneous effects of chemotherapy in CLL, in particular that fludarabine therapy can achieve lasting remission in IGHV-M, but not in IGHV-U patients.

Beyond TLR, trisomy 12 modulated a broad range of stimulus responses and drug-stimulus interactions, comparable to the impact of IGHV status. Molecularly, we link the observed trisomy 12 phenotype to higher activity of Spi-B and PU.1, essential regulators of environmental sensing in B-cells[41]. Our observation that Spi-B and PU.1 are essential for proliferation in lymphoma cell lines highlights the potential importance of these TFs in survival and proliferation particularly in trisomy 12 CLL.

We present a data resource for the study of CLL drug response in the context of cell-intrinsic and cell-extrinsic modulators. The data may inform targeted mechanistic investigations[47] and direct efforts for combination therapies. The entire dataset, including the reproducible analysis, can be downloaded from the online repository (github.com/Huber-group-EMBL/CLLCytokineScreen2021), or explored interactively (imbi.uni-heidelberg.de/dietrichlab/CLL_Microenvironment/).

Acknowledgments

We thank the Department of Medicine V, University of Heidelberg, Molecular Medicine Partnership Unit (MMPU), EMBL Heidelberg and DKFZ/Heidelberg Center for Personalized Oncology (DKFZ/HIPO) for technical support and funding. HG was supported by a Joachim-Herz Add-on Fellowship for Interdisciplinary Science. PB was supported by a doctoral scholarship of the Franziska-Kolb foundation. S.D. was supported by the Else Kröner Fresenius Foundation, the German Federal Ministry of Education and Research (SYMPATHY) and the German Research Foundation (SFB873). J.L., S.D. and W.H. were supported by the German Federal Ministry of Education and Research (CompLS project MOFA under grant agreement number 031L0171A). T.R. was supported by a physician scientist fellowship of the Medical Faculty of University Heidelberg and the German Federal Ministry of Education and Research (CompLS project SIMONA under grant agreement number 031L0263A). For experimental technical support and expertise, we thank Mareike Knoll, Angela Lenze, Brian Lai, and Vladimir Benes and Nayara Trevisan Doimo de Azevedohe of the EMBL Genomics Core Facility. We thank EMBL's IT Services for providing data management and computing infrastructure, and Simone Bell for organisational support. We thank Mike Smith and Frederik Ziebell for advice on statistics and analysis, Martina Seiffert for the HS-5 stromal cell line, and Michael Boutros, Moritz Gerstung, Nassos Typas and Simon Anders for their comments on the manuscript and their valued advice.

P.M.B is a MD candidate at the University of Heidelberg. This work is submitted in partial fulfillment of the requirement for the MD. H.A.R.G is a PhD candidate for the joint PhD degree between EMBL and Heidelberg University, Faculty of Biosciences. This work is submitted in partial fulfillment of the requirement for the PhD.

Author contributions

S.D. and P.-M.B, designed the experiments. S.D., W.H., H.A.R.G. and P.-M.B, conceptualised the data analysis. W.H. and S.D. supervised the study. W.H., T.Z. and S.D. conceptualised the multi-omics approach to analyse CLL drug response. P.-M.B, performed the drug-stimulus

profiling experiments with support from C.K., S.S. and L.W.. T.Z., C.M.T. and P.D. provided guidance on experimental protocols. H.A.R.G., P.M.B, J.H., J.L., S.D. performed data processing and curation. H.A.R.G. and P.-M.B, analysed and interpreted the data, with support from W.H., S.D., J.L, S.H. and T.R., and produced the figures with input from W.H. and S.D.. H.A.R.G. performed statistical inference and regression modelling, P.-M.B, performed exploratory analysis and integration with clinical data. T.B. and S.H. performed the shRNA knockdown experiments, J.B.Z. and I.B. provided the ATACseq dataset used in Figure 4 and quantified differential transcription factor activity, M.K., K.K. and C.Z. generated the immunohistochemistry data, and P.-M.B, analysed these data. H.A.R.G. designed and wrote the Shiny app and the software documentation. P.-M.B, and H.A.R.G. wrote the manuscript, with input from S.D. and W.H.. All authors reviewed and edited the manuscript.

Conflict of Interest Disclosures

The authors declare that they have no conflict of interests.

References

1. Bruch P-M, Giles H, Kolb C, et al. Systematic investigation of microenvironmental drug resistance mechanisms in chronic Lymphocytic leukemia. *Blood*. 2019;134(Supplement_1):3363–3363.
2. Fabbri G, Dalla-Favera R. The molecular pathogenesis of chronic lymphocytic leukaemia. *Nat. Rev. Cancer*. 2016;16(3):145–162.
3. Puente XS, Jares P, Campo E. Chronic lymphocytic leukemia and mantle cell lymphoma: crossroads of genetic and microenvironment interactions. *Blood*. 2018;131(21):2283–2296.
4. Burger JA, Tedeschi A, Barr PM, et al. Ibrutinib as Initial Therapy for Patients with Chronic Lymphocytic Leukemia. *N. Engl. J. Med.* 2015;373(25):2425–2437.
5. Fischer K, Al-Sawaf O, Bahlo J, et al. Venetoclax and Obinutuzumab in Patients with CLL and Coexisting Conditions. *N. Engl. J. Med.* 2019;380(23):2225–2236.

6. Gaidano G, Rossi D. The mutational landscape of chronic lymphocytic leukemia and its impact on prognosis and treatment. *Hematology Am. Soc. Hematol. Educ. Program*. 2017;2017(1):329–337.
7. Döhner H, Stilgenbauer S, Benner A, et al. Genomic aberrations and survival in chronic lymphocytic leukemia. *N. Engl. J. Med.* 2000;343(26):1910–1916.
8. Strefford JC. The genomic landscape of chronic lymphocytic leukaemia: biological and clinical implications. *Br. J. Haematol.* 2015;169(1):14–31.
9. Herndon TM, Chen S-S, Saba NS, et al. Direct in vivo evidence for increased proliferation of CLL cells in lymph nodes compared to bone marrow and peripheral blood. *Leukemia*. 2017;31(6):1340–1347.
10. Collins RJ, Verschuer LA, Harmon BV, et al. Spontaneous programmed death (apoptosis) of B-chronic lymphocytic leukaemia cells following their culture in vitro. *Br. J. Haematol.* 1989;71(3):343–350.
11. Oppermann S, Ylanko J, Shi Y, et al. High-content screening identifies kinase inhibitors that overcome venetoclax resistance in activated CLL cells. *Blood*. 2016;128(7):934–947.
12. Ten Hacken E, Burger JA. Microenvironment interactions and B-cell receptor signaling in Chronic Lymphocytic Leukemia: Implications for disease pathogenesis and treatment. *Biochim. Biophys. Acta*. 2016;1863(3):401–413.
13. Ahn IE, Farooqui MZH, Tian X, et al. Depth and durability of response to ibrutinib in CLL: 5-year follow-up of a phase 2 study. *Blood*. 2018;131(21):2357–2366.
14. Chen Z, ter Burg H, Andrejeva G, et al. LINKING MICROENVIRONMENTAL SIGNALS TO METABOLIC SWITCHES AND IBRUTINIB RESPONSE IN CHRONIC LYMPHOCYTIC LEUKEMIA: PS1125. *HemaSphere*. 2019;3:509–510.
15. Aguilar-Hernandez MM, Blunt MD, Dobson R, et al. IL-4 enhances expression and function of surface IgM in CLL cells. *Blood*. 2016;127(24):3015–3025.
16. Jayappa KD, Portell CA, Gordon VL, et al. Microenvironmental agonists generate phenotypic resistance to combined ibrutinib plus venetoclax in CLL and MCL. *Blood*

Adv. 2017;1(14):933–946.

17. Chatzouli M, Ntoufa S, Papakonstantinou N, et al. Heterogeneous functional effects of concomitant B cell receptor and TLR stimulation in chronic lymphocytic leukemia with mutated versus unmutated Ig genes. *J. Immunol.* 2014;192(10):4518–4524.
18. Dietrich S, Krämer OH, Hahn E, et al. Leflunomide induces apoptosis in fludarabine-resistant and clinically refractory CLL cells. *Clin. Cancer Res.* 2012;18(2):417–431.
19. Carey A, Edwards DK, Eide CA,et al. Identification of Interleukin-1 by Functional Screening as a Key Mediator of Cellular Expansion and Disease Progression in Acute Myeloid Leukemia. *Cell Rep.* 2017;18(13):3204–3218.
20. Dietrich S, Oleś M, Lu J, et al. Drug-perturbation-based stratification of blood cancer. *J. Clin. Invest.* 2018;128(1):427–445.
21. Libregts SF, Gutiérrez L, de Bruin AM, et al. Chronic IFN-γ production in mice induces anemia by reducing erythrocyte life span and inhibiting erythropoiesis through an IRF-1/PU.1 axis. *Blood*. 2011;118(9):2578–2588.
22. Lenz G, Wright GW, Emre NCT, et al. Molecular subtypes of diffuse large B-cell lymphoma arise by distinct genetic pathways. *Proc. Natl. Acad. Sci. U. S. A.* 2008;105(36):13520–13525.
23. Bankhead P, Loughrey MB, Fernández JA, et al. QuPath: Open source software for digital pathology image analysis. *Sci. Rep.* 2017;7(1):1–7.
24. Love MI, Huber W, Anders S. Moderated estimation of fold change and dispersion for RNA-seq data with DESeq2. *Genome Biol.* 2014;15(12):550.
25. Therneau TM, Grambsch PM. Modeling Survival Data: Extending the Cox Model. Springer Science & Business Media; 2000.
26. Friedman J, Hastie T, Tibshirani R. Regularization Paths for Generalized Linear Models via Coordinate Descent. *J. Stat. Softw.* 2010;33(1):1–22.
27. Wilkerson MD, Hayes DN. ConsensusClusterPlus: a class discovery tool with confidence assessments and item tracking. *Bioinformatics*. 2010;26(12):1572–1573.
28. Yu G, Wang L-G, Han Y, He Q-Y. clusterProfiler: an R Package for Comparing

Biological Themes Among Gene Clusters. *OMICS: A Journal of Integrative Biology*. 2012;16(5):284–287.

29. Yu G, Wang L-G, He Q-Y. ChIPseeker: an R/Bioconductor package for ChIP peak annotation, comparison and visualization. *Bioinformatics*. 2015;31(14):2382–2383.
30. Akalin A, Franke V, Vlahoviček K, Mason CE, Schübeler D. Genomation: a toolkit to summarize, annotate and visualize genomic intervals. *Bioinformatics*. 2015;31(7):1127–1129.
31. Malgorzata Oles, Sascha Dietrich, Junyan Lu, Britta Velten, Andreas Mock, Vladislav Kim, Wolfgang Huber. BloodCancerMultiOmics2017. Bioconductor; 2018.
32. Rendeiro AF, Schmidl C, Strefford JC, et al. Chromatin accessibility maps of chronic lymphocytic leukaemia identify subtype-specific epigenome signatures and transcription regulatory networks. *Nat. Commun.* 2016;7:11938.
33. Berest I, Arnold C, Reyes-Palomares A, et al. Quantification of Differential Transcription Factor Activity and Multiomics-Based Classification into Activators and Repressors: diffTF. *Cell Rep.* 2019;29(10):3147–3159.e12.
34. Kulakovskiy IV, Vorontsov IE, Yevshin IS, et al. HOCOMOCO: expansion and enhancement of the collection of transcription factor binding sites models. *Nucleic Acids Res.* 2016;44(D1):D116–25.
35. Care MA, Cocco M, Laye JP, et al. SPIB and BATF provide alternate determinants of IRF4 occupancy in diffuse large B-cell lymphoma linked to disease heterogeneity. *Nucleic Acids Res.* 2014;42(12):7591–7610.
36. Edgar R, Domrachev M, Lash AE. Gene Expression Omnibus: NCBI gene expression and hybridization array data repository. *Nucleic Acids Res.* 2002;30(1):207–210.
37. Baumann T, Moia R, Gaidano G, et al. Lymphocyte doubling time in chronic lymphocytic leukemia modern era: a real-life study in 848 unselected patients. *Leukemia*. 2021;
38. Garrett-Sinha LA, Dahl R, Rao S, Barton KP, Simon MC. PU.1 exhibits partial functional redundancy with Spi-B, but not with Ets-1 or Elf-1. *Blood*. 2001;97(9):2908–2912.
39. Turkistany SA, DeKoter RP. The Transcription Factor PU.1 is a Critical Regulator of

Cellular Communication in the Immune System. *Arch. Immunol. Ther. Exp.* . 2011;59(6):431–440.

40. Ray-Gallet D, Mao C, Tavitian A, Moreau-Gachelin F. DNA binding specificities of Spi-1/PU.1 and Spi-B transcription factors and identification of a Spi-1/Spi-B binding site in the c-fes/c-fps promoter. *Oncogene*. 1995;11(2):303–313.
41. Willis SN, Tellier J, Liao Y, et al. Environmental sensing by mature B cells is controlled by the transcription factors PU.1 and SpiB. *Nat. Commun.* 2017;8(1):1426.
42. Hayden RE, Pratt G, Roberts C, Drayson MT, Bunce CM. Treatment of chronic lymphocytic leukemia requires targeting of the protective lymph node environment with novel therapeutic approaches. *Leuk. Lymphoma*. 2012;53(4):537–549.
43. Mittal AK, Chaturvedi NK, Rai KJ, et al. Chronic lymphocytic leukemia cells in a lymph node microenvironment depict molecular signature associated with an aggressive disease. *Mol. Med.* 2014;20:290–301.
44. Yan X-J, Dozmorov I, Li W, et al. Identification of outcome-correlated cytokine clusters in chronic lymphocytic leukemia. *Blood*. 2011;118(19):5201–5210.
45. Roider T, Seufert J, Uvarovskii A, et al. Dissecting intratumour heterogeneity of nodal B-cell lymphomas at the transcriptional, genetic and drug-response levels. *Nature Cell Biology*. 2020;22(7):896–906.
46. Spaner DE, McCaw L, Wang G, Tsui H, Shi Y. Persistent janus kinase-signaling in chronic lymphocytic leukemia patients on ibrutinib: Results of a phase I trial. *Cancer Med.* 2019;8(4):1540–1550.
47. Lu J, Cannizzaro E, Meier-Abt F, et al. Multi-omics reveals clinically relevant proliferative drive associated with mTOR-MYC-OXPHOS activity in chronic lymphocytic leukemia. *Nat Cancer*. 2021;

Figure Legends

Figure 1. Study outline and overview of drugs and stimuli.

(A) Schematic of experimental protocol. By combining 12 drugs and 17 stimuli, we systematically queried the effects of simultaneous stimulation and inhibition of critical pathways in CLL (n=192). Integrating functional drug-stimulus response profiling with four additional omics layers, we identified pro-survival pathways, underlying molecular modulators of drug and microenvironment reponses, and drug-stimulus interactions in CLL. All screening data can be explored either manually (github.com/Huber-group-EMBL/CLLCytokineScreen2021 or interactively, via the shiny app (www.imbi.uni-heidelberg.de/dietrichlab/CLL_Microenvironment/). (B) Overview of stimuli included in the screen and summary of their associated targets. HS-5 Culture Medium is omitted, as no specific target can be shown. (C) Table of drugs included in the screen. Drug target, and category of target are also shown. (D and E) Forest plots of Pearson coefficients calculated from selected pairwise drug-drug (D) and stimulus-stimulus (E) correlations. Closely related stimuli targeting the NfKB and JAK-STAT pathways are shown as examples of stimuli which share very similar receptors and downstream target profiles but show a divergence of effects.

Figure 2. Ex vivo cell viability assay of CLL primary samples reveals subgroups with distinct stimulus response profiles, and differential disease progression.

(A) The heatmap matrix shows the viability measurements for 192 samples (columns) and 17 stimuli (rows). Viability was measured via ATP-based assay after 48h stimulation. The data are shown normalised to DMSO-treated controls, and scaled within each row according to the Median Absolute Deviation. Limits were applied to scaling factor for optimal visualisation. The colour bars to the right show sample annotations. Consensus Clustering was used to define column tree layout, using hierarchical clustering with the Euclidean metric. (B) Lymphocyte doubling time, a clinical marker for disease progression, plotted for each cluster. (C) Kaplan-

Meier curves of time to next treatment for each cluster. p-values from univariate Cox proportional hazard models comparing IGHV-U enriched C1 with C2, and IGHV-M enriched C3 with C4. (D) Multinomial regression with lasso penalisation to identify enrichment or depletion of genetic features within each cluster. Matrix of genetic features (p=39), and IGHV status (encoded as M = 1 and U = 0) were used to identify multivariate predictors of cluster assignment. x axis shows genetic predictors, y axis indicates value and sign of coefficient assigned to feature, for each cluster (positive coefficients are enriched in the cluster, negative coefficients are depleted). Coefficients shown are mean coefficients from 50 bootstrapped repeats and error bars represent the mean ± standard deviation. Genetic features with >20% missing values were excluded, and only patients with complete annotation were included in the model (n=137). (E) Gene set enrichment analysis (GSEA) to compare expression of genes in samples from C3 and C4 reveals upregulation of Hallmark pathways involved in microenvironmental signalling, stress response, metabolism and proliferation in C3. Normalised enrichment scores are shown for top 10 most significant pathways upregulated in C3 versus C4. Bars coloured according to adjusted p-value. Genes are ranked based on Wald statistic, calculated using the Deseq2 package and GSEA performed using the fgsea algorithm.

Figure 3. Responses to microenvironmental signals are modulated by genetic alterations recurrent in CLL.

(A) Overview of results of all tested gene - stimulus associations. x-axis shows stimuli, y-axis shows p-values from Student's t-test (two-sided, with equal variance). Tests were performed for somatic mutations and copy number aberrations present in ≥3 patients, and IGHV status (n = 63). Each circle represents a gene-stimulus association. Tests with p-values smaller than the threshold corresponding to a false discovery rate (FDR) of 10% (method of Benjamini and Hochberg) are indicated by colored circles, where the colors represent the gene mutations and structural aberrations. (B) Predictor profiles for selected stimuli to represent gene - stimulus associations identified through Gaussian linear modelling with L1-penalty. Matrix of genetic

features (p=39), IGHV status (encoded as M = 1 and U = 0), and Methylation Cluster (encoded as 0, 0.5, 1) were used to identify multivariate predictors. Bar plots on left indicate size and sign of coefficients assigned to the named predictors. Positive coefficients indicate higher viability after stimulation if the feature is present. Scatter plot and heatmap indicate how each genetic feature relates to sample viabilities: Scatter plots indicate log(viability) values, in order of magnitude, for each individual sample. Heatmaps show mutation status for each of the genetic predictors for corresponding sample in scatter plot. Coefficients for sCD40L + IL4 and CpG ODN were also significant, these plots have been omitted to avoid redundancy.

Figure 4. Trisomy 12 modulates responses to microenvironmental signals.

(A) Trisomy 12 IGHV-M samples show a strongly positive reaction to TLR stimulation, comparable to IGHV-U samples. Plot shows log transformed viability values, normalised to DMSO controls, after stimulation with the TLR 7/8 agonist Resiquimod. p-values from Student's t-test. (B) Spi-B and PU.1 TF binding sites show higher accessibility in trisomy 12 CLL. Bar plot shows change in TF activity (y axis) between between trisomy 12 (n = 9) and non-trisomy 12 samples (n = 43), for all significant TFs (x axis, adjusted p-value <0.05). Data taken from Rendeiro et al 2016[32], and change in TF activity calculated using the diffTF package, and measured as weighted mean difference. p-values are obtained through diffTF in permutation mode and adjusted by the Benjamini-Hochberg procedure. TF binding sites and names from HOCOMOCO database. (C) ChIPseq analysis of Spi-B and PU.1 binding indicates involvement in coordinating transcriptional response to microenvironmental signals, including TLR. Table shows results from over-representation tests of selected KEGG and Reactome pathways amongst Spi-B and PU.1 targets. Columns show geneset pathways, corresponding database, the number of genes within geneset, the number of Spi-B and PU.1 target genes within geneset (total number of target genes defined also shown), and p-value from over-representation test. TF targets defined as closest gene to each significant ChIP peak (q value<0.05), and within ±1kb of TSS. ChIPseq data from Care et al. 2014[28]. Over-representation tests run using clusterProfiler package, method corresponds to one-sided

version of Fisher's exact test. (D) Knockdown of Spi-B and PU.1 led to growth restriction and cell death. Data shown is the mean of three technical replicates. While SU-DHL 5 was already growth impaired after Spi-B KD, SU-DHL 2 and SU-DHL 4 were only impaired after double knock-down. Double knockdown lead to rapid cell death in SU-DHL 5 (data not shown). Cell count normalised to seeded cell number of diffuse large b cell lymphoma cell lines after knockdown of Spi-B or double knockdown of Spi-B and PU.1 or shRNA as control.

Figure 5. Signals from the microenvironment influence ex-vivo drug response.

(A) Graphical representation of the four drug - stimulus interaction categories. Categories are defined according to the nature of the interaction (synergistic or antagonistic), and whether the viability is increased or decreased by the stimulus (positive or negative). x-axis shows treatment type, y-axis shows viability with each treatment. Points (red) depict a representative treatment response pattern for given interaction type. To demonstrate the effect of each interaction on expected viability, blue and black horizontal lines represent the expected viability for combinatorial treatment in the absence of an interaction between drug - stimulus (blue) and the viability for combinatorial treatment with given interaction (black). (B) Histogram to show the number of drug- stimulus interactions within each category, where p value for β_{int} is <0.05. (C) Heatmap of all β_{int} values for all drug - stimulus combinations where p for β_{int} <0.05, annotated with interaction type. Scale indicates size and sign of β_{int}. Rows and columns clustered according to hierarchical clustering. (D - I) Examples of drug-stimulus interactions, for each category. Plots show log transformed viability values with each treatment, for all samples. Matching samples are linked across treatments. Black and blue horizontal lines indicate the predicted viability from the linear model for each single and combinatorial treatment. In combinatorial treatment, both the expected viability based on the additive effect of drug and stimulus (blue), and the viability with interaction (black) are shown, to indicate the impact of the interaction. (D+E) Ibrutinib, a clinically-used BTK inhibitor, is blocked by IL4 and IFNγ. (F) The JAK inhibitor pyridone-6 inhibits the pro-survival effect of sCD40L + IL4 stimulation. (G) The p38 inhibitor ralimetinib and IFNγ show a synergistic pro-survival effect

not seen in either single treatment. (H) TLR agonists, including CpG ODN (shown) increase sensitivity to BTK inhibition by ibrutinib, despite increasing viability in isolation. (I) Soluble anti-IgM sensitises CLL samples to HSP90 inhibition by luminespib.

Figure 6. Integrating the effects of genetic features and stimuli on drug response. (A) Representative predictor profile depicting genetic features that modulate the size of β_{int} between fludarabine and CpG ODN, to illustrate the approach used. To generate predictor profile, linear model in Eqn. (1) was fitted in a sample - specific manner, to calculate drug-stimulus interaction coefficients (β_{int}) for each patient sample. Ranked patient-specific β_{int} values are shown in lower scatter plot. Associations between the size of β_{int} and genetic features were identified using multivariate regression with L1 (lasso) regularisation, with gene mutations (p = 39) and IGHV status as predictors, and selecting coefficients that were chosen in >90% of bootstrapped model fits. The horizontal bars on left show the size of fitted coefficients assigned to genetic features. Matrix above scatter plot indicates patient mutation status for the selected genetic features. Matrix fields correspond to points in scatter plot (ie patient data is aligned), to indicate how the size of β_{int} varies with selected genetic feature. Grey lines indicate presence of genetic feature/IGHV mutated. (B) Heatmap depicting overview of genetic predictors of drug - stimulus interactions (each row represents the coefficients from fitting a single multivariate model, as in (A)). Stimuli are shown on left, and corresponding drugs on right. Coloured fields indicate that β_{int} for given drug and stimulus is modulated by corresponding genetic feature. Positive coefficients are shown in red, indicating a more positive β_{int} if the feature is present. Only top 8 most commonly selected genetic features are shown. Drug - stimulus combinations with no genetic predictors of β_{int} amongst top 8 shown are omitted for clarity. (C-D) Beeswarm boxplots of log(viability) values, for (C) fludarabine and CpG ODN and (D) ibrutinib and IL4 single and combinatorial treatments, faceted by IGHV status and trisomy 12 status. P-values from paired Student's t-tests.

Figure 7. IL4 and TLR signaling are upregulated in CLL-infiltrated lymph nodes.

Lymph node biopsies of CLL-infiltrated and non-neoplastic samples were stained for pSTAT6, a downstream target of IL4, and pIRAK4, a downstream target of TLR, revealing increased signaling activity in CLL-infiltrated lymph nodes. (A-B) Mean pSTAT6 and pIRAK4 staining intensity after background substraction (y axis), p values from Student's t-test. (C-F) Example images of IHC sections. (C, D) shows pSTAT6 levels in (C) CLL-infiltrated and (D) non-neoplastic samples. (E,F) shows pIRAK4 levels in (E) CLL-infiltrated and (F) non-neoplastic samples. (G-H) Kaplan-Meier plots for treatment free survival stratified by levels (high / low) of pSTAT6 (G) and pIRAK4 (H). The two pSTAT6 and pIRAK4 groups were defined by mean staining intensities dichotomised using maximally selected rank statistics. The same 64 CLL lymph node samples were used for both Kaplan-Meier plots. 50 patient samples were in the high pSTAT6 group, and 52 in the high pIRAK4 group.

A

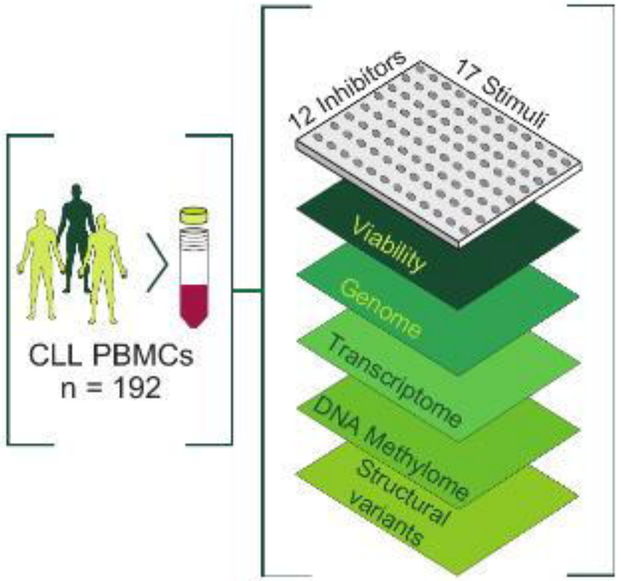

B

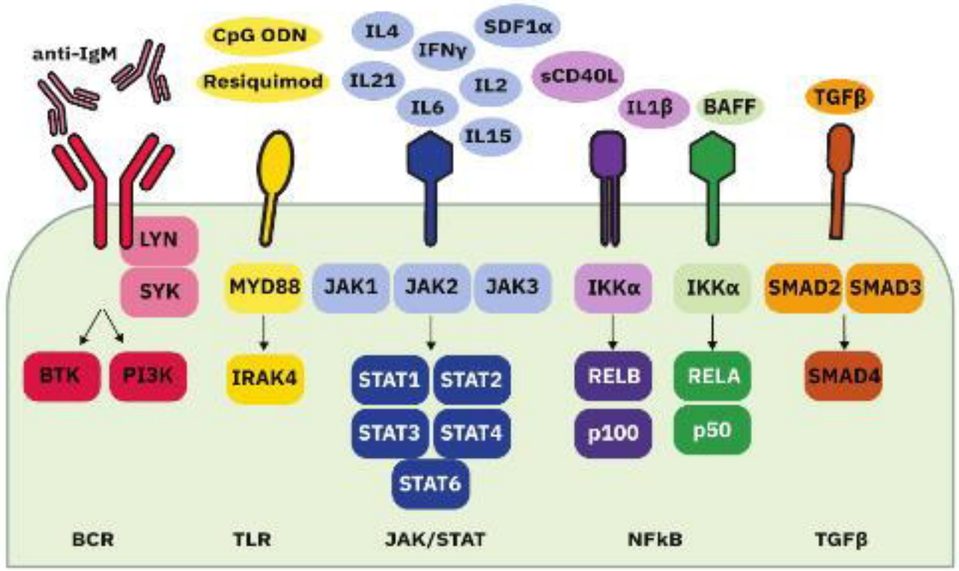

C

Drug	Target	Category
Ibrutinib	BTK	BCR
Idelalisib	PI3K delta	BCR
PRT062607	SYK	BCR
Fludarabine	Purine analogue	DDR
Nutlin-3a	MDM2	DDR
I-BET 762	BRD2/3/4	Epigenome
Luminespib	HSP90	HSP90
Pyridone-6	JAK1/2/3	JAK/STAT
Selumetinib	MEK1/2	MAPK
Ralimetinib	p38 MAPK	MAPK
Everolimus	mTOR	mTOR
BAY-11-7085	NFkB	NFkB

D

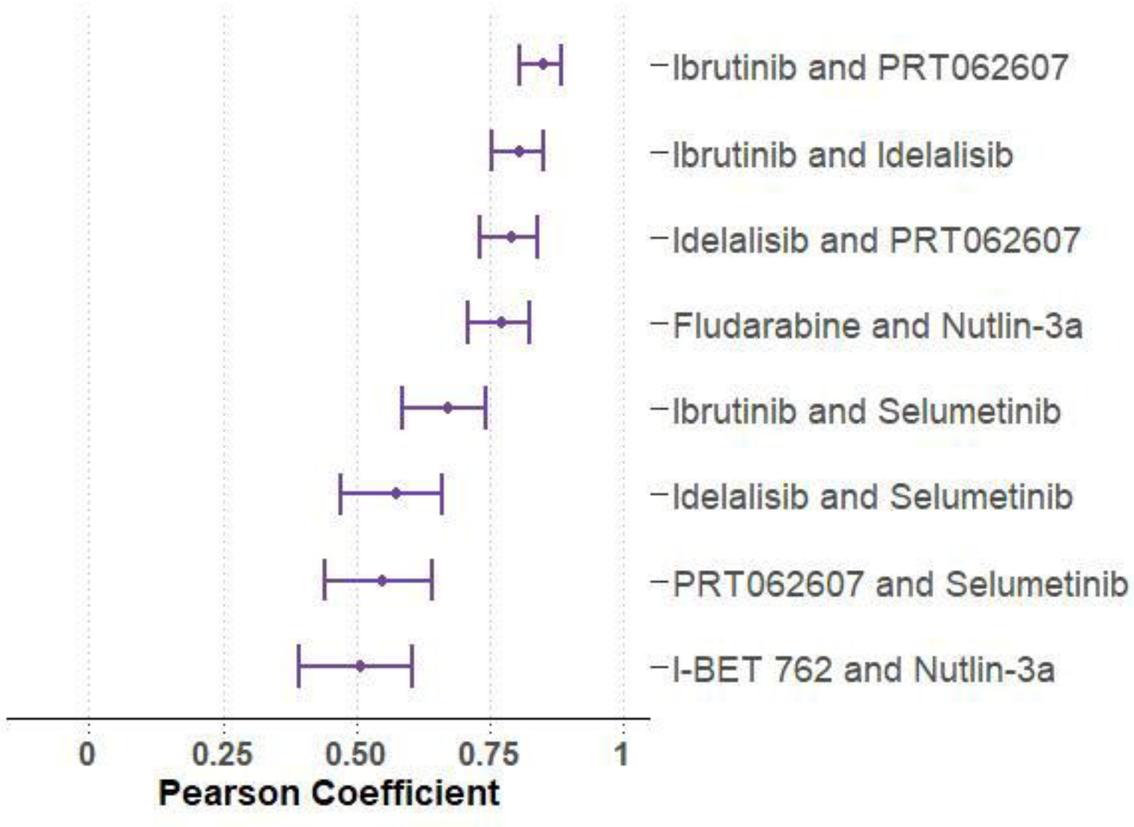

E

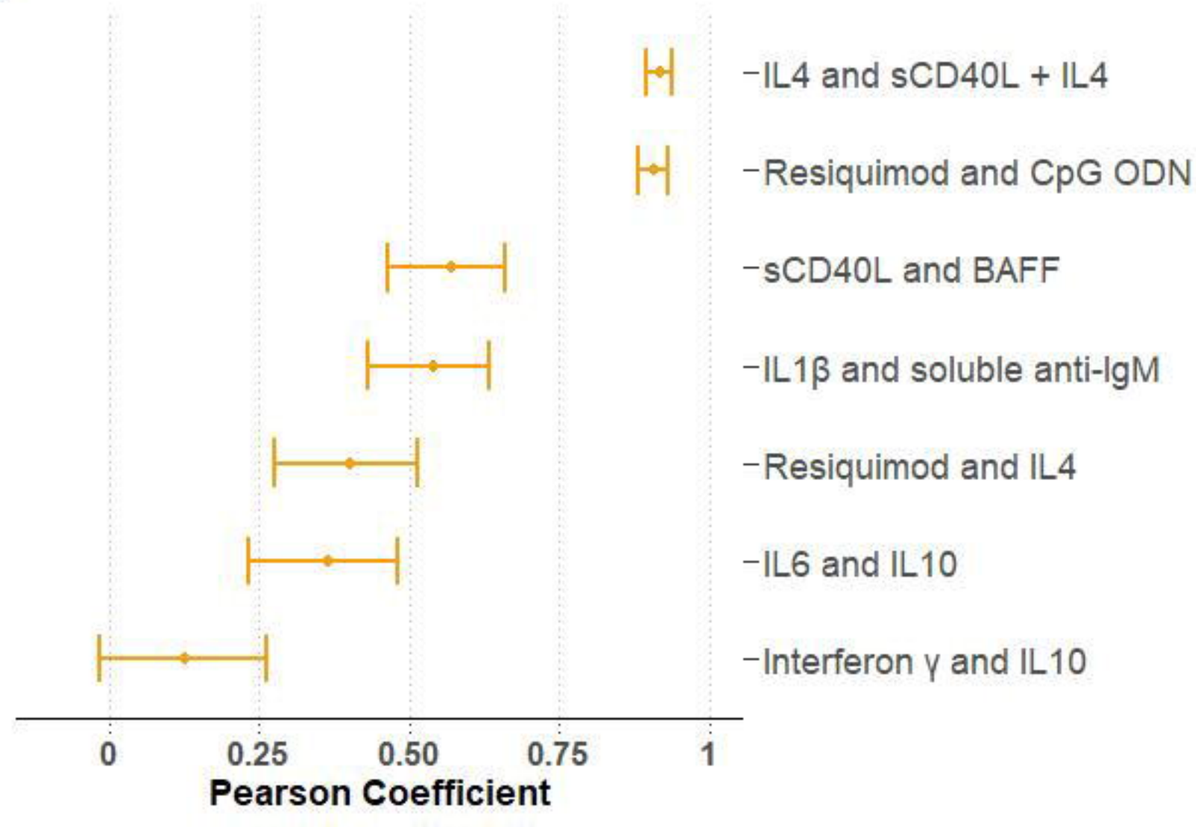

A

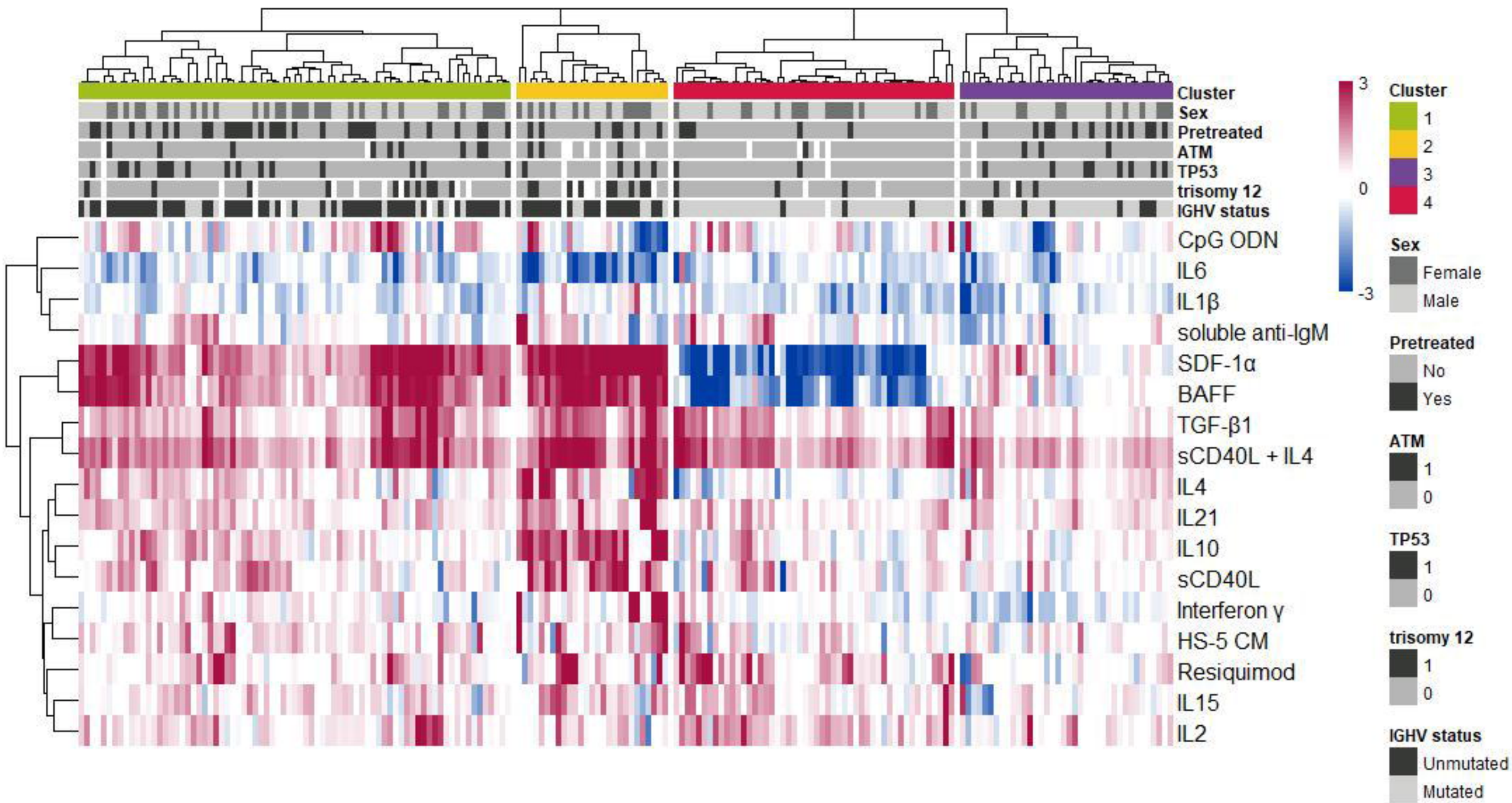
Cluster
Sex
Pretreated
ATM
TP53
trisomy 12
IGHV status
CpG ODN
IL6
IL1β
soluble anti-IgM
SDF-1α
BAFF
TGF-β1
sCD40L + IL4
IL4
IL21
IL10
sCD40L
Interferon γ
HS-5 CM
Resiquimod
IL15
IL2
3
0
-3
Cluster
1
2
3
4
Sex
Female
Male
Pretreated
No
Yes
ATM
1
0
TP53
1
0
trisomy 12
1
0
IGHV status
Unmutated
Mutated

B

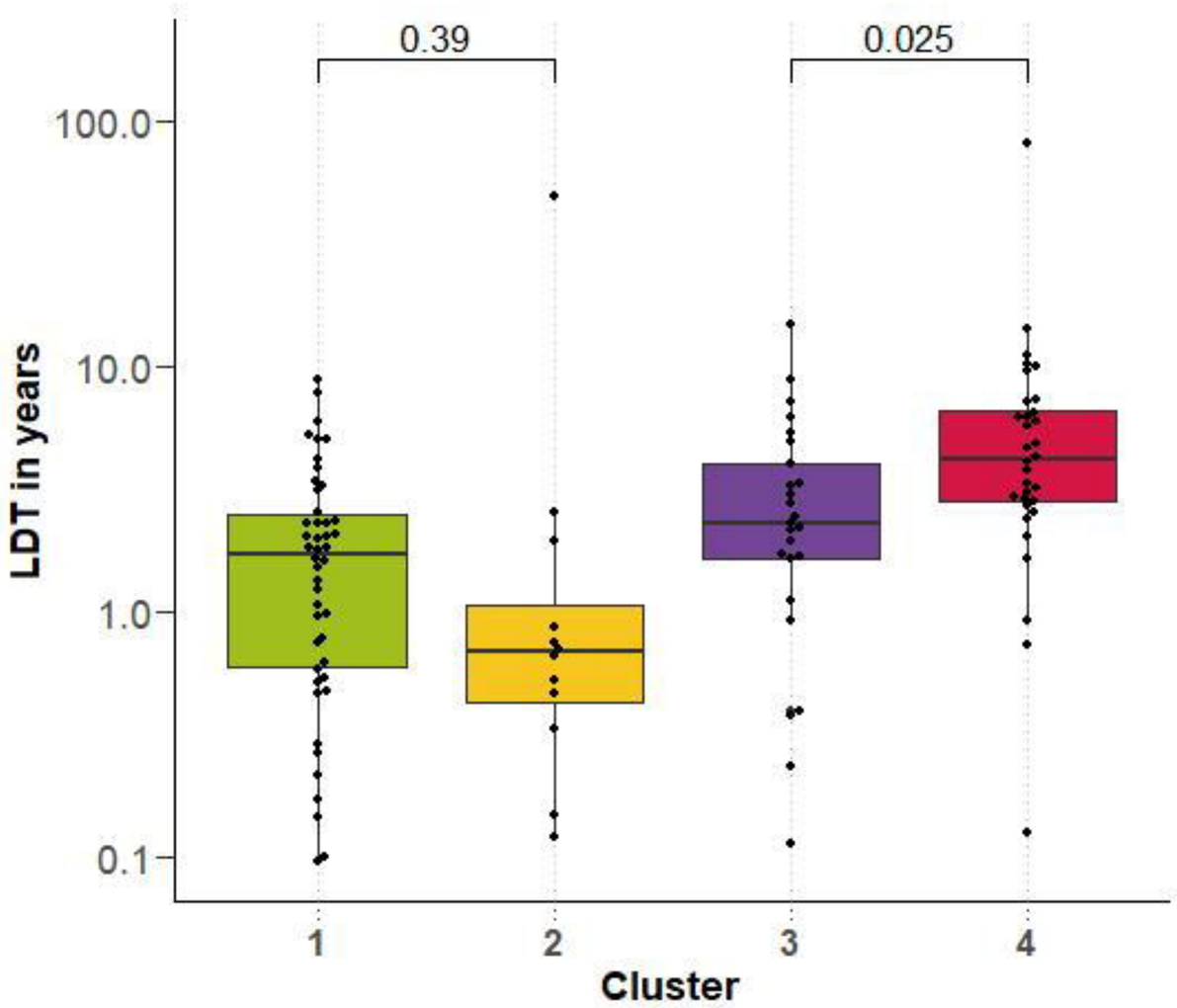
0.39
0.025
100.0
10.0
1.0
0.1
LDT in years
1
2
3
4
Cluster

C

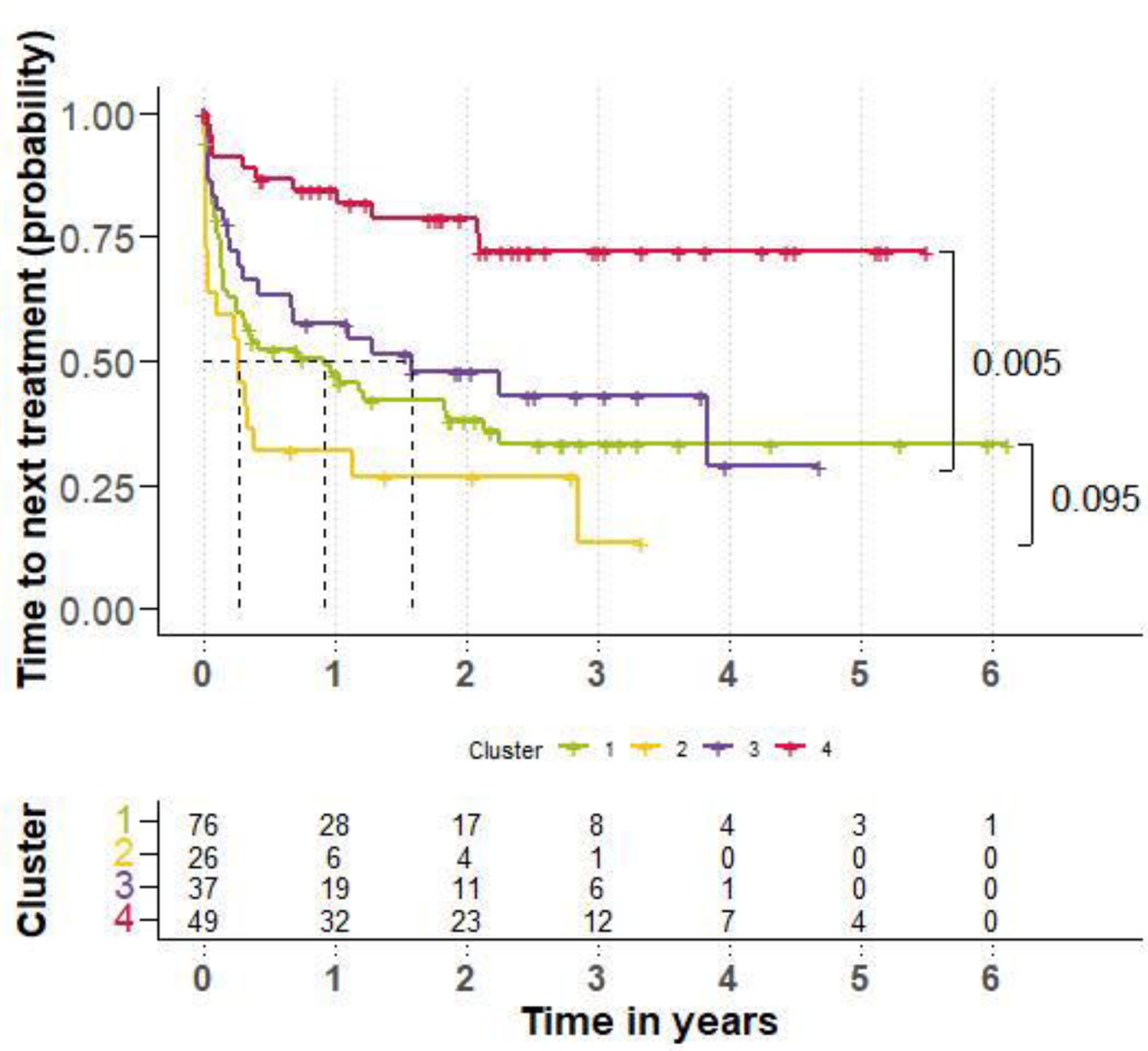
Time to next treatment (probability)
1.00
0.75
0.50
0.25
0.00
0.005
0.095
0
1
2
3
4
5
6
Cluster 1 2 3 4
Cluster
1 76 28 17 8 4 3 1
2 26 6 4 1 0 0 0
3 37 19 11 6 1 0 0
4 49 32 23 12 7 4 0
Time in years

D

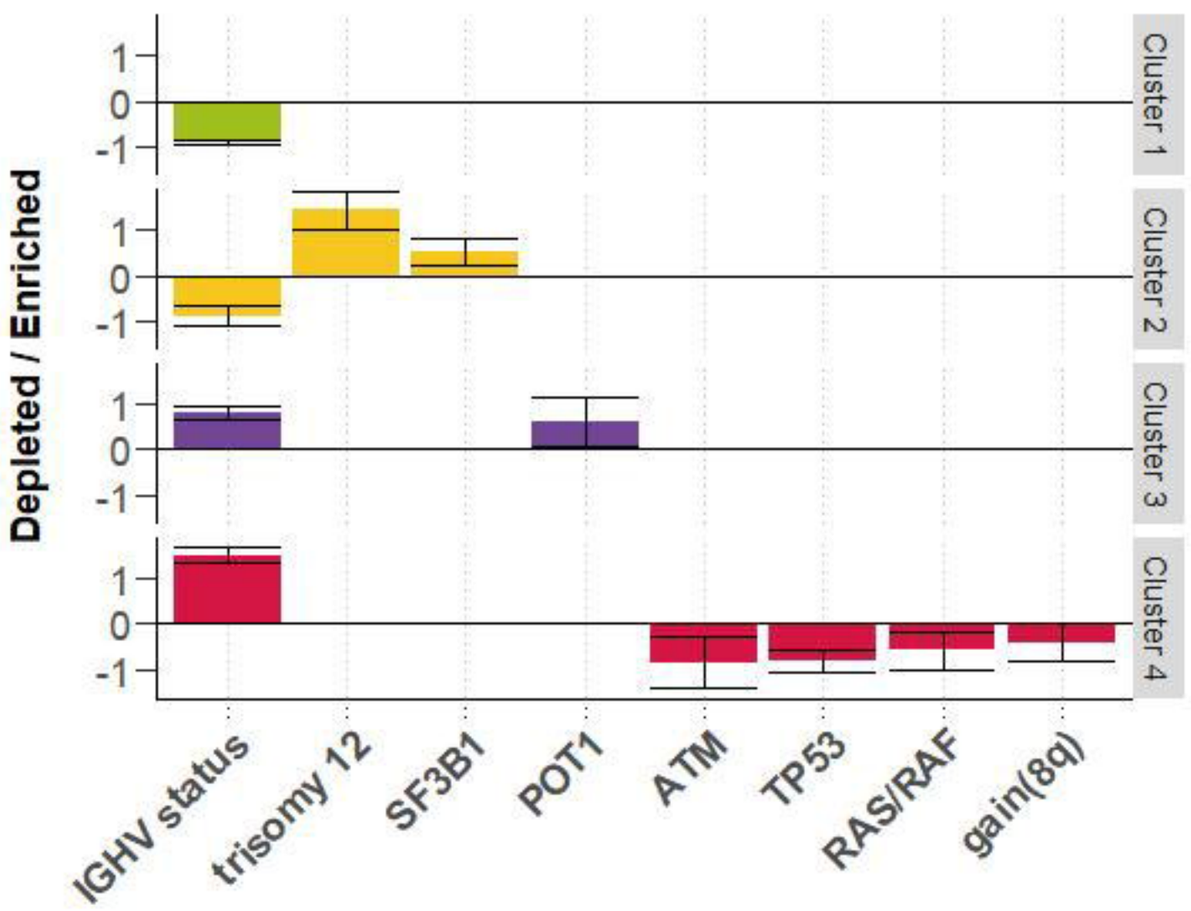
Depleted / Enriched
1
0
-1
Cluster 1
Cluster 2
Cluster 3
Cluster 4
IGHV status
trisomy 12
SF3B1
POT1
ATM
TP53
RAS/RAF
gain(8q)

E

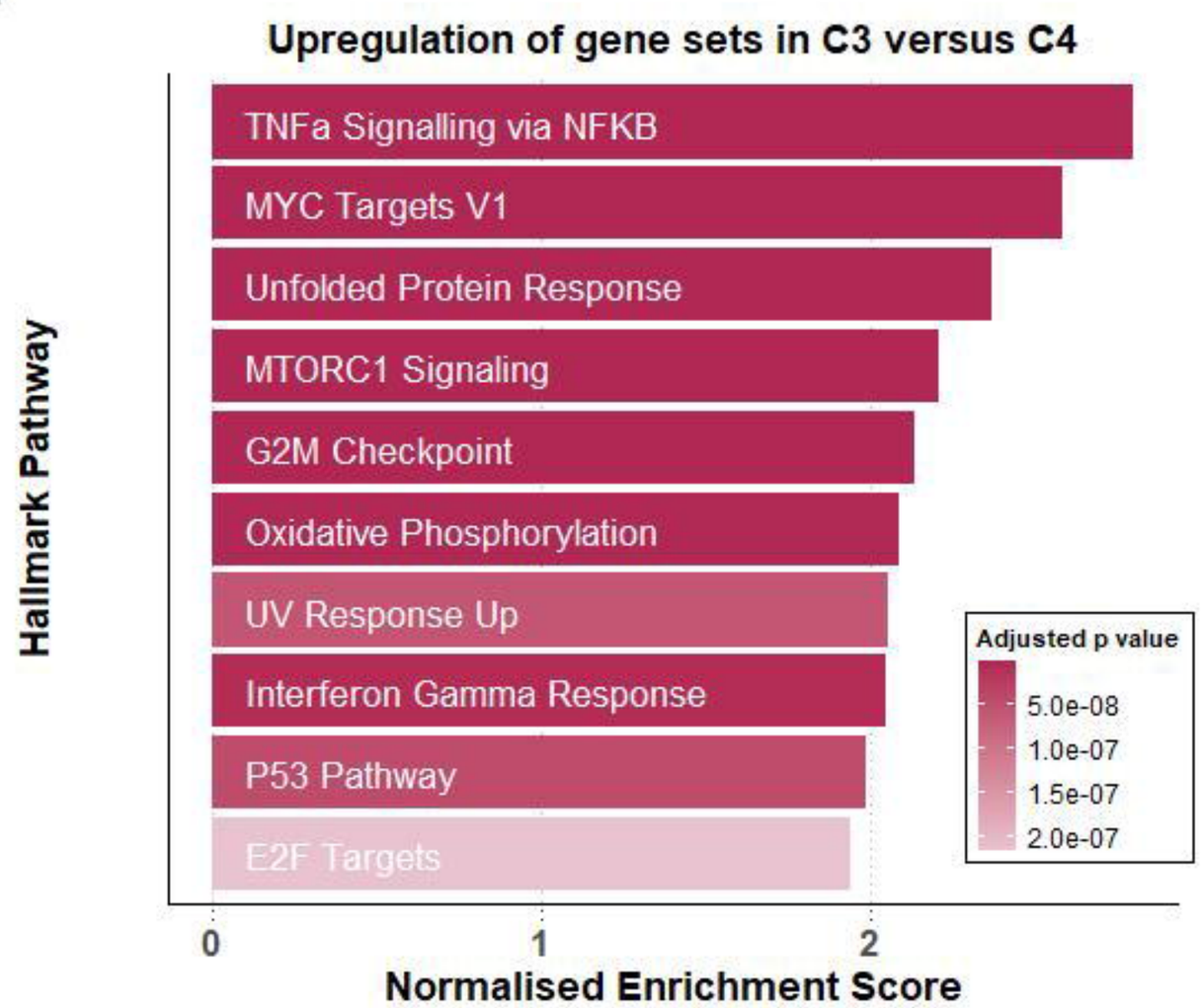
Upregulation of gene sets in C3 versus C4
Hallmark Pathway
TNFa Signalling via NFKB
MYC Targets V1
Unfolded Protein Response
MTORC1 Signaling
G2M Checkpoint
Oxidative Phosphorylation
UV Response Up
Interferon Gamma Response
P53 Pathway
E2F Targets
Adjusted p value
5.0e-08
1.0e-07
1.5e-07
2.0e-07
0
1
2
Normalised Enrichment Score

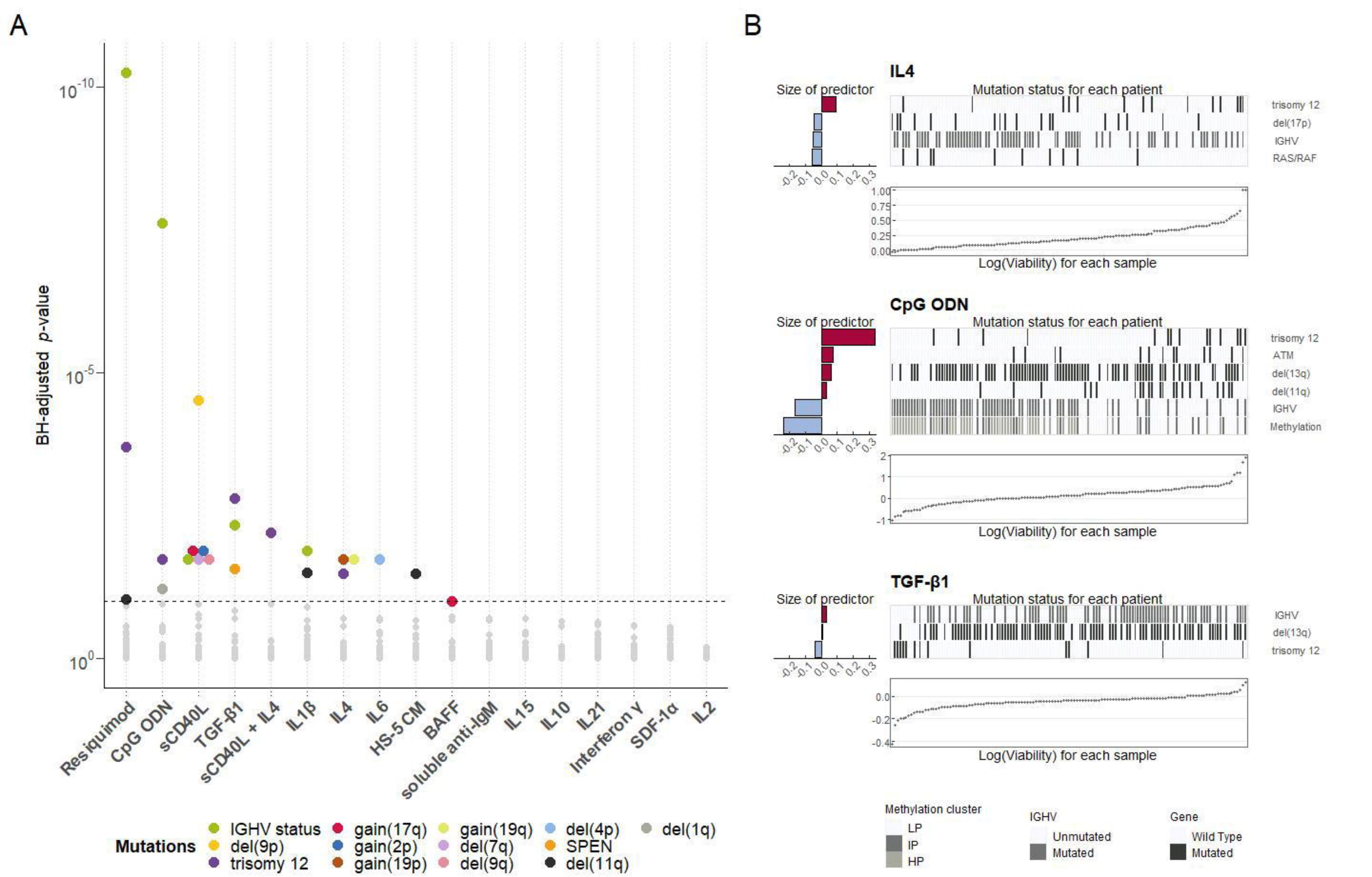

A
B
BH-adjusted p-value
10^-10
10^-5
10^0
Resiquimod
CpG ODN
sCD40L
TGF-β1
sCD40L + IL4
IL1β
IL4
IL6
HS-5 CM
BAFF
soluble anti-IgM
IL15
IL10
IL21
Interferon γ
SDF-1α
IL2
Mutations
IGHV status
del(9p)
trisomy 12
gain(17q)
gain(2p)
gain(19p)
gain(19q)
del(7q)
del(9q)
del(4p)
SPEN
del(11q)
del(1q)
IL4
Size of predictor
Mutation status for each patient
trisomy 12
del(17p)
IGHV
RAS/RAF
Log(Viability) for each sample
CpG ODN
Size of predictor
Mutation status for each patient
trisomy 12
ATM
del(13q)
del(11q)
IGHV
Methylation
Log(Viability) for each sample
TGF-β1
Size of predictor
Mutation status for each patient
IGHV
del(13q)
trisomy 12
Log(Viability) for each sample
Methylation cluster
LP
IP
HP
IGHV
Unmutated
Mutated
Gene
Wild Type
Mutated

A

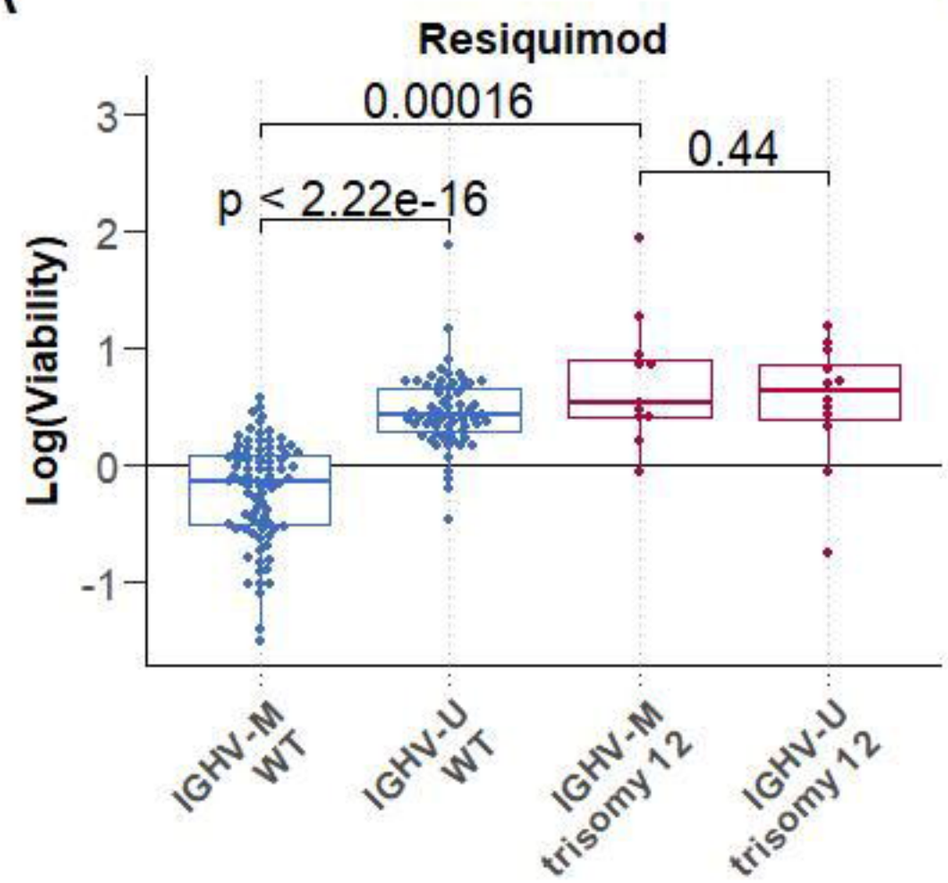

B

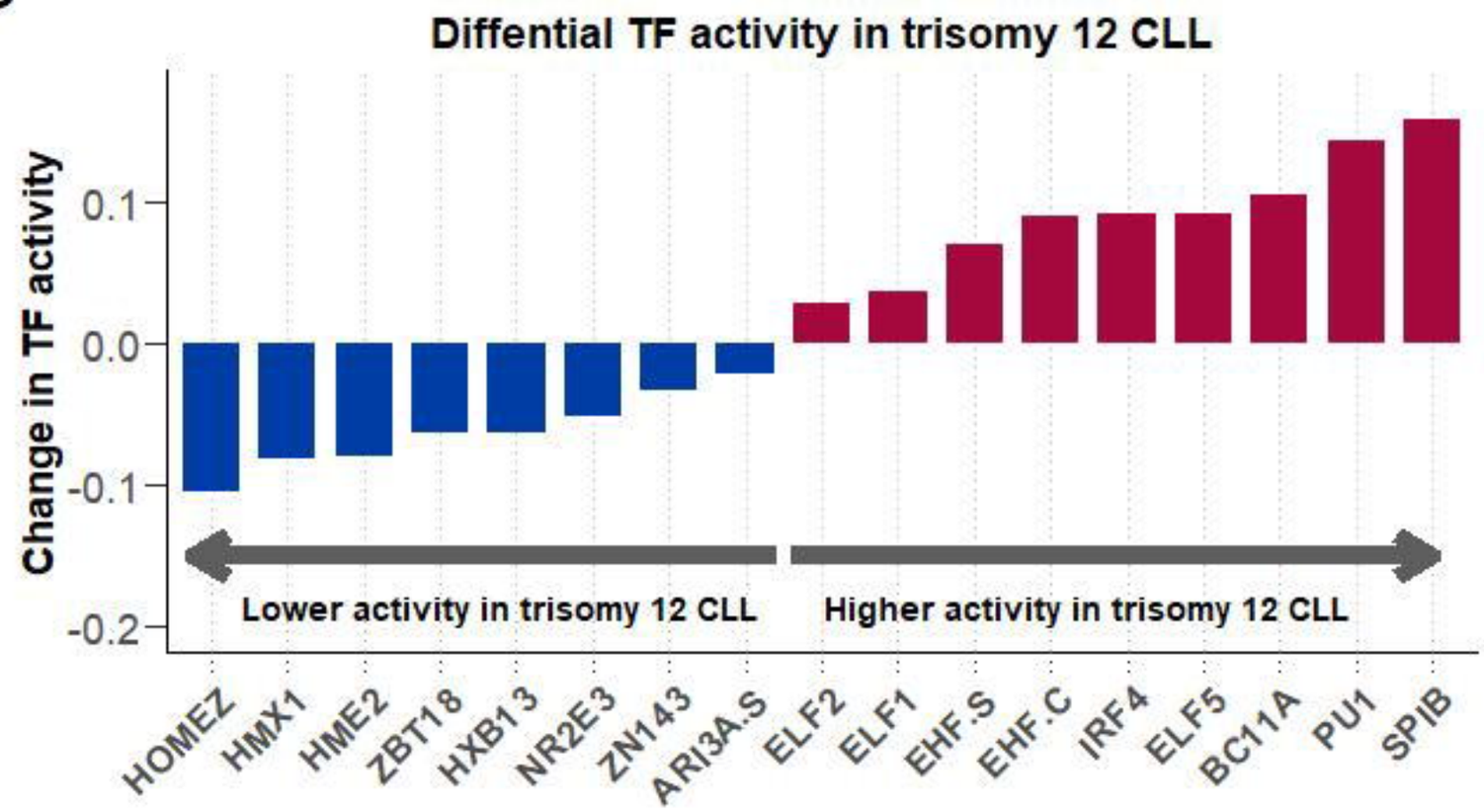

C

Pathway	Geneset Database	Geneset Size	Spi-B targets (/3253)	SPIB p-value	PU.1 targets (/250)	PU1 p-value
BCR Signaling Pathway	KEGG	75	36	0.000	4	0.056
TLR Signaling Pathway	KEGG	102	40	0.000	5	0.046
Signaling by TGFbeta Receptor Complex	Reactome	73	26	0.007	0	1.000

D

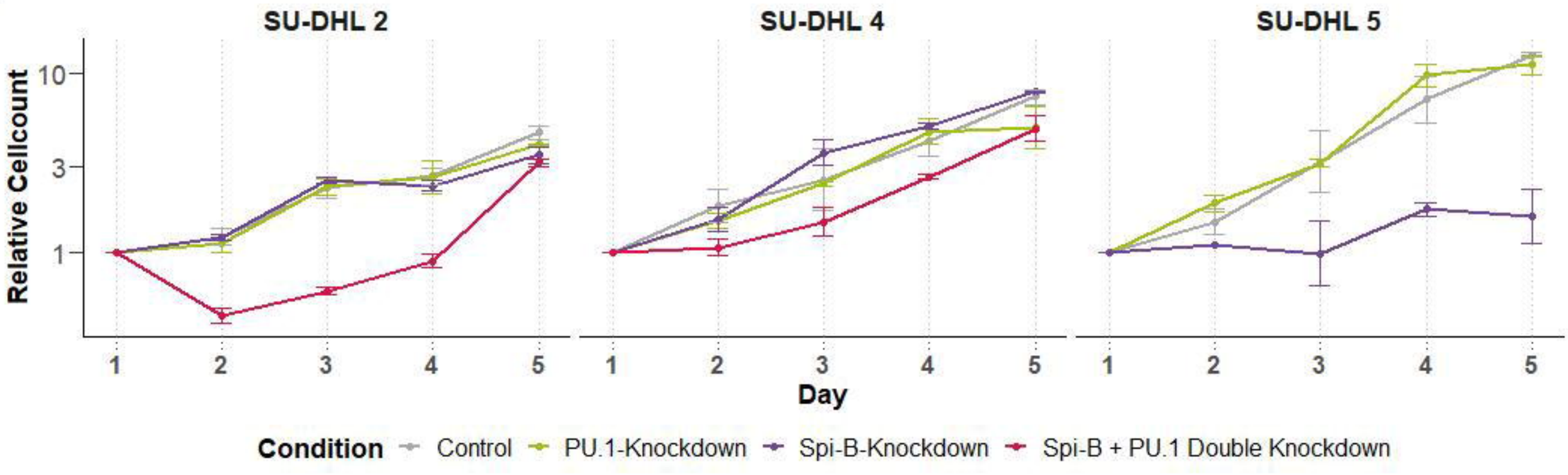

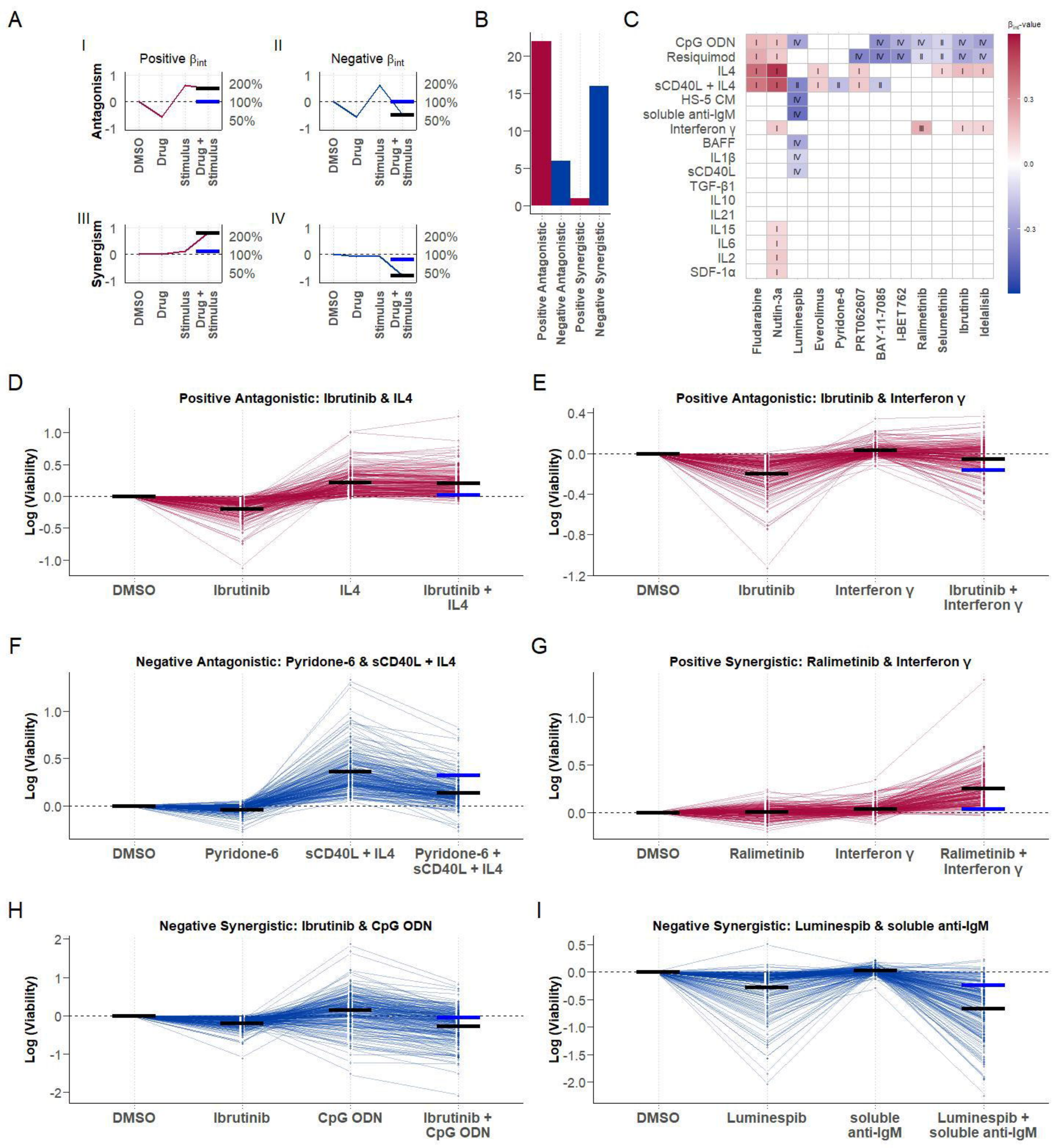
A
I
Positive β_{int}
Antagonism
II
Negative β_{int}
III
Synergism
IV
200%
100%
50%
DMSO
Drug
Stimulus
Drug + Stimulus
B
Positive Antagonistic
Negative Antagonistic
Positive Synergistic
Negative Synergistic
C
β_{int}-value
CpG ODN
Resiquimod
IL4
sCD40L + IL4
HS-5 CM
soluble anti-IgM
Interferon γ
BAFF
IL1β
sCD40L
TGF-β1
IL10
IL21
IL15
IL6
IL2
SDF-1α
Fludarabine
Nutlin-3a
Luminespib
Everolimus
Pyridone-6
PRT062607
BAY-11-7085
I-BET 762
Ralimetinib
Selumetinib
Ibrutinib
Idelalisib
D
Positive Antagonistic: Ibrutinib & IL4
Log (Viability)
DMSO
Ibrutinib
IL4
Ibrutinib + IL4
E
Positive Antagonistic: Ibrutinib & Interferon γ
Interferon γ
Ibrutinib + Interferon γ
F
Negative Antagonistic: Pyridone-6 & sCD40L + IL4
Pyridone-6
sCD40L + IL4
Pyridone-6 + sCD40L + IL4
G
Positive Synergistic: Ralimetinib & Interferon γ
Ralimetinib
Ralimetinib + Interferon γ
H
Negative Synergistic: Ibrutinib & CpG ODN
CpG ODN
Ibrutinib + CpG ODN
I
Negative Synergistic: Luminespib & soluble anti-IgM
Luminespib
soluble anti-IgM
Luminespib + soluble anti-IgM

A

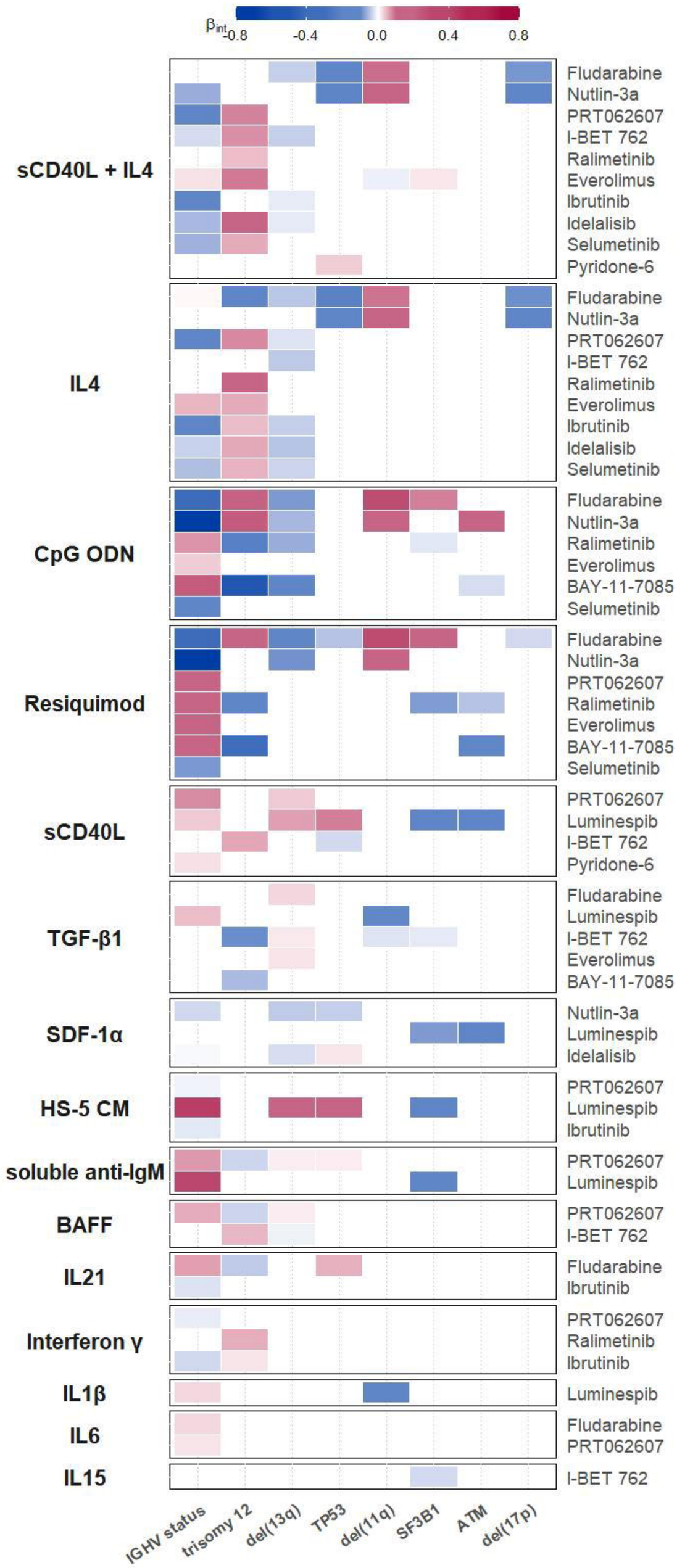
βint
-0.8
-0.4
0.0
0.4
0.8
sCD40L + IL4
Fludarabine
Nutlin-3a
PRT062607
I-BET 762
Ralimetinib
Everolimus
Ibrutinib
Idelalisib
Selumetinib
Pyridone-6
IL4
Fludarabine
Nutlin-3a
PRT062607
I-BET 762
Ralimetinib
Everolimus
Ibrutinib
Idelalisib
Selumetinib
CpG ODN
Fludarabine
Nutlin-3a
Ralimetinib
Everolimus
BAY-11-7085
Selumetinib
Resiquimod
Fludarabine
Nutlin-3a
PRT062607
Ralimetinib
Everolimus
BAY-11-7085
Selumetinib
sCD40L
PRT062607
Luminespib
I-BET 762
Pyridone-6
TGF-β1
Fludarabine
Luminespib
I-BET 762
Everolimus
BAY-11-7085
SDF-1α
Nutlin-3a
Luminespib
Idelalisib
HS-5 CM
PRT062607
Luminespib
Ibrutinib
soluble anti-IgM
PRT062607
Luminespib
BAFF
PRT062607
I-BET 762
IL21
Fludarabine
Ibrutinib
Interferon γ
PRT062607
Ralimetinib
Ibrutinib
IL1β
Luminespib
IL6
Fludarabine
PRT062607
IL15
I-BET 762
IGHV status
trisomy 12
del(13q)
TP53
del(11q)
SF3B1
ATM
del(17p)

B

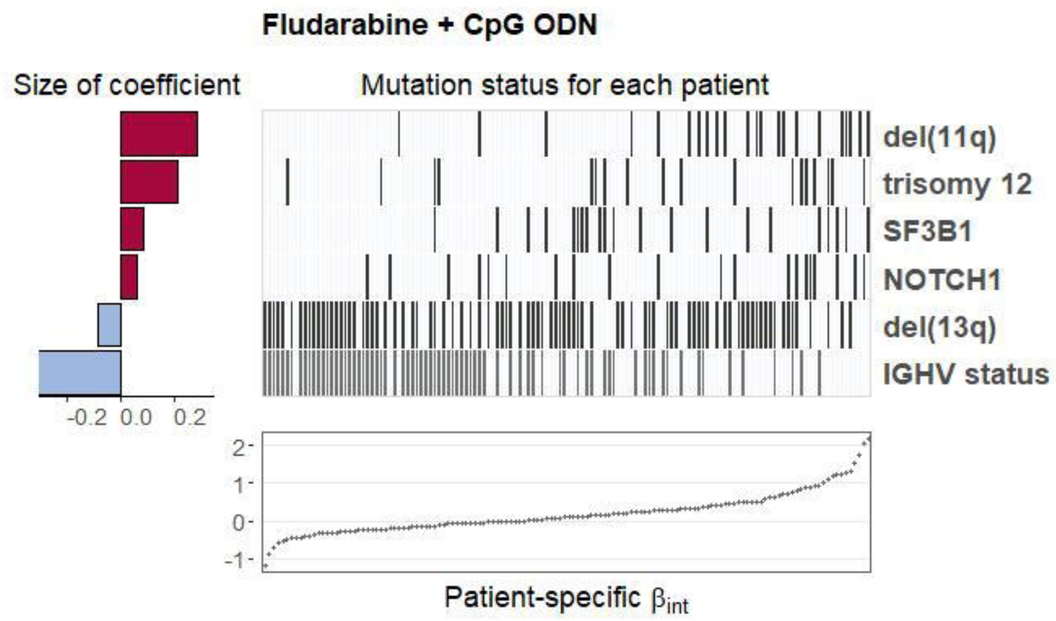
Fludarabine + CpG ODN
Size of coefficient
Mutation status for each patient
-0.2
0.0
0.2
del(11q)
trisomy 12
SF3B1
NOTCH1
del(13q)
IGHV status
2
1
0
-1
Patient-specific βint

C

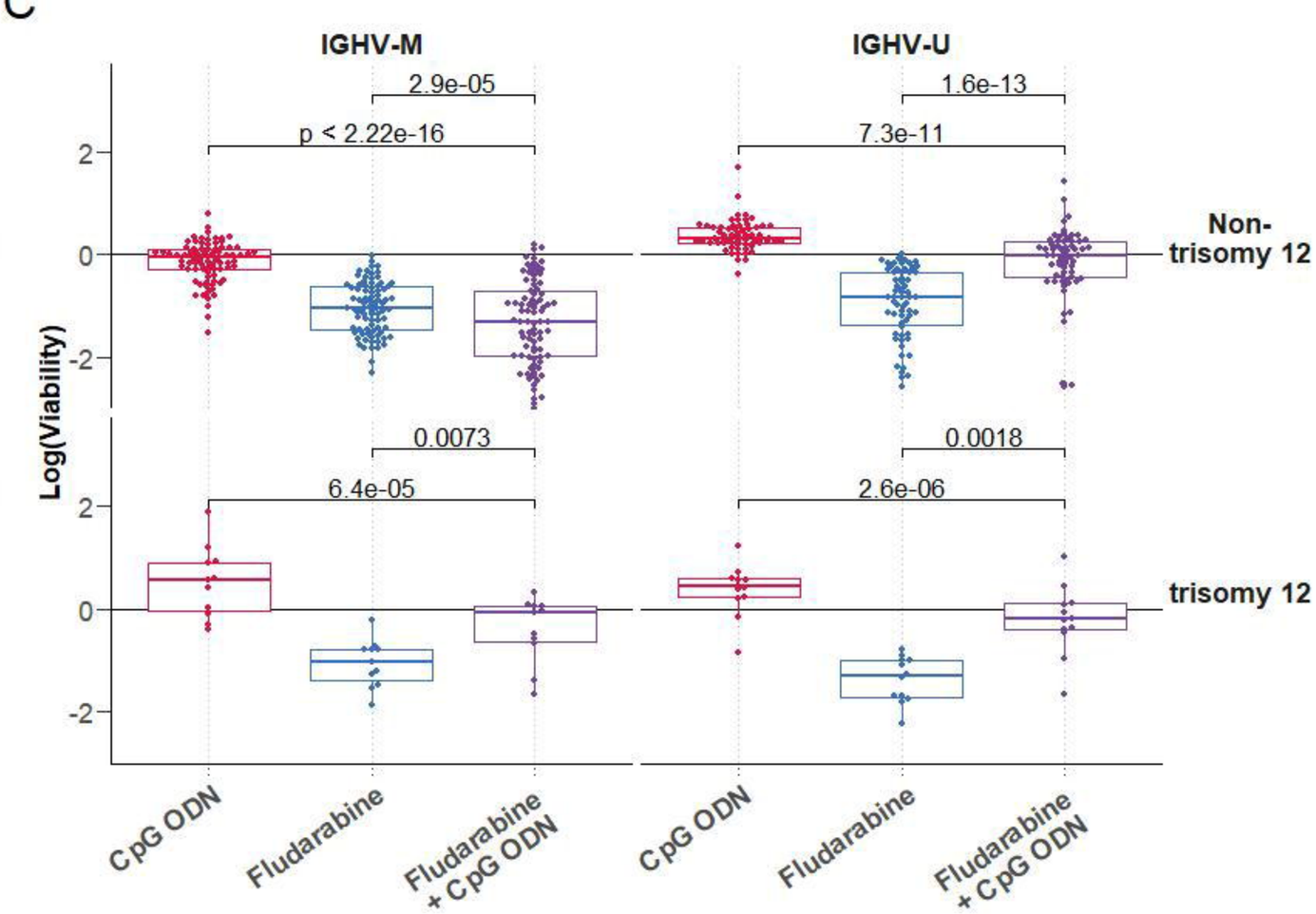
IGHV-M
IGHV-U
2.9e-05
p < 2.22e-16
1.6e-13
7.3e-11
0.0073
6.4e-05
0.0018
2.6e-06
Log(Viability)
Non-trisomy 12
trisomy 12
CpG ODN
Fludarabine
Fludarabine + CpG ODN

D

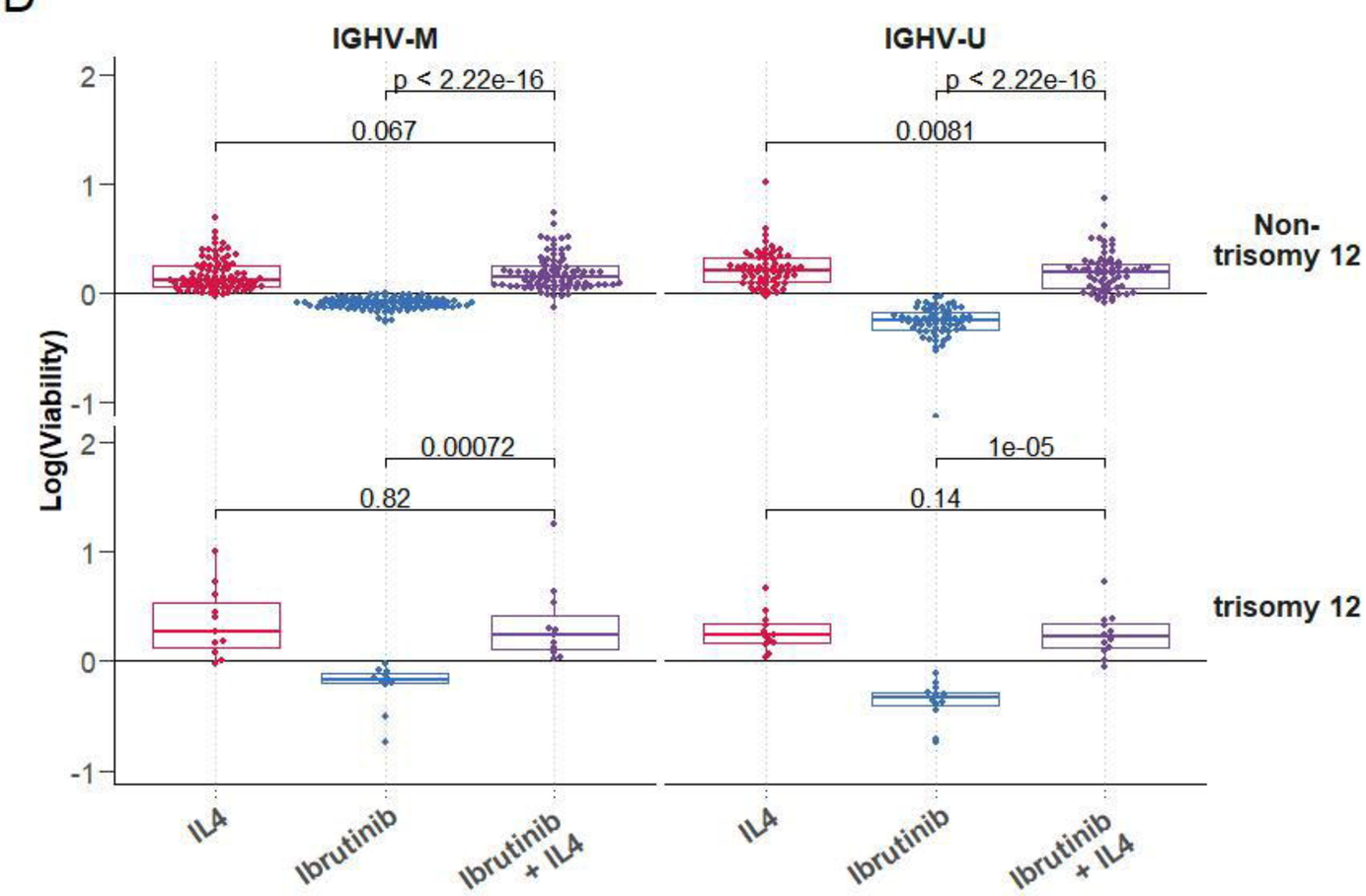
IGHV-M
IGHV-U
p < 2.22e-16
0.067
0.0081
0.00072
0.82
1e-05
0.14
Log(Viability)
Non-trisomy 12
trisomy 12
IL4
Ibrutinib
Ibrutinib + IL4

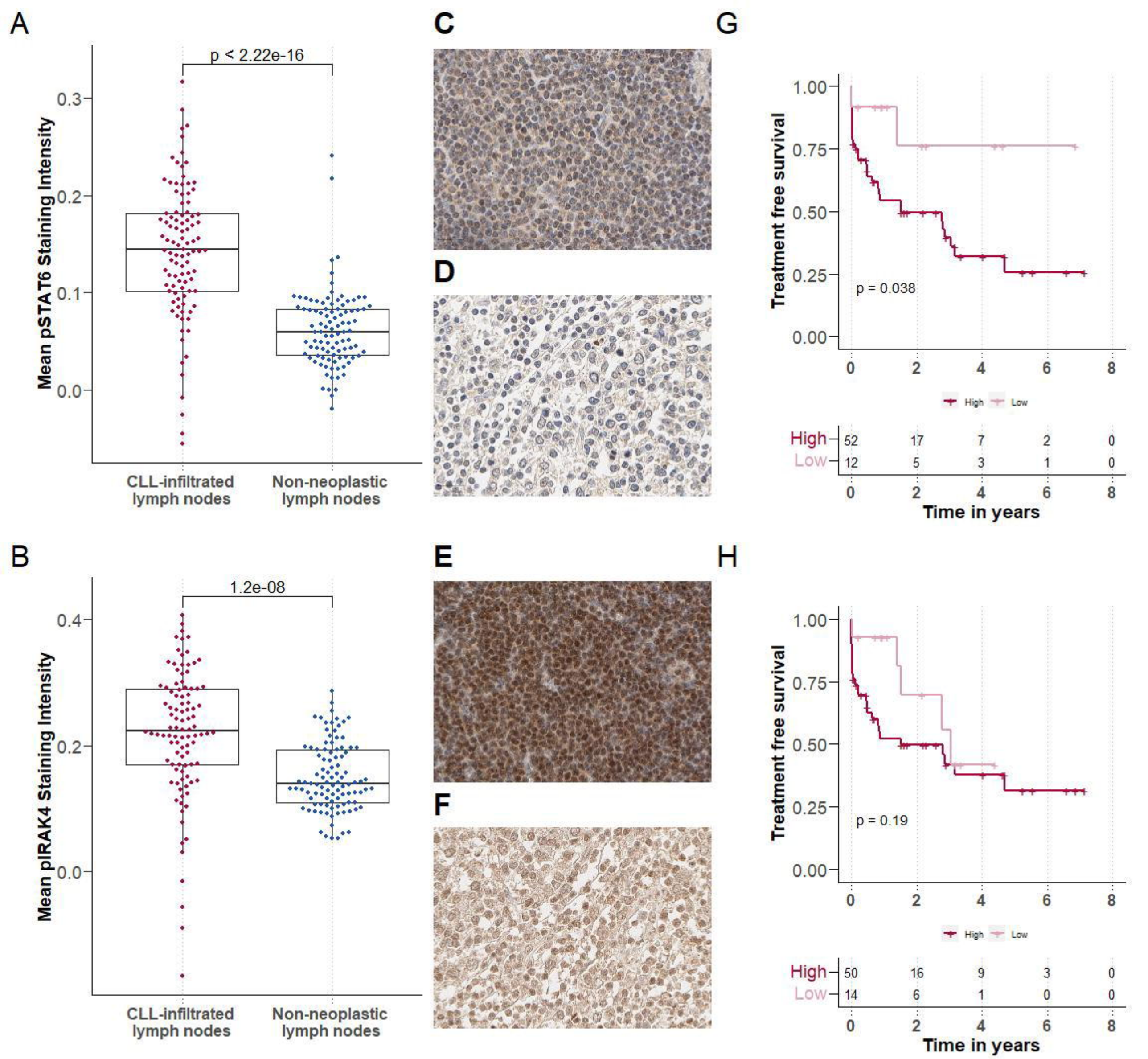
A
p < 2.22e-16
Mean pSTAT6 Staining Intensity
0.3
0.2
0.1
0.0
CLL-infiltrated lymph nodes
Non-neoplastic lymph nodes
C
D
G
Treatment free survival
1.00
0.75
0.50
0.25
0.00
p = 0.038
0
2
4
6
8
High
Low
52 17 7 2 0
12 5 3 1 0
Time in years
B
1.2e-08
Mean pIRAK4 Staining Intensity
0.4
0.2
0.0
CLL-infiltrated lymph nodes
Non-neoplastic lymph nodes
E
F
H
Treatment free survival
1.00
0.75
0.50
0.25
0.00
p = 0.19
0
2
4
6
8
High
Low
50 16 9 3 0
14 6 1 0 0
Time in years